Palaeogeography, Palaeoclimatology, Palaeoecology 459 (2016) 99–120

Contents lists available at ScienceDirect

Palaeogeography, Palaeoclimatology, Palaeoecology

journal homepage: www.elsevier.com/locate/palaeo

Mineral and chemostratigraphy of a Toarcian black shale hosting Mn-carbonate microbialites (Úrkút, Hungary)

Márta Polgári [b,*], James R. Hein [c], Lóránt Bíró [a], Ildikó Gyollai [a], Tibor Németh [a], Csanád Sajgó [a], József Fekete [a], Lorenz Schwark [d], Elemér Pál-Molnár [e], Mária Hámor-Vidó [a], Tamás Vigh [f]

[a] Research Center for Astronomy and Geosciences, Geobiomineralization and Astrobiological Research Group, Institute for Geology and Geochemistry, Hungarian Academy of Sciences, Budapest, Budaörsi str. 45, 1112 Budapest, Hungary
[b] Eszterházy Károly College, Dept. of Natural Geography and Geoinformatics, Leányka str. 6, 3300 Eger, Hungary
[c] USGS, 2885 Mission St., Santa Cruz, CA 95060, USA
[d] CAU, Kiel, Germany
[e] Szeged University, Dept. of Mineralogy, Geochemistry and Petrology, Egyetem str. 2-6, 6702 Szeged, Hungary
[f] Mangán Ltd, Külterület 1, Úrkút 8409, Hungary,

ARTICLE INFO

Article history:
Received 19 April 2016
Received in revised form 15 June 2016
Accepted 19 June 2016
Available online 23 June 2016

Keywords:
T-OAE
Mn-carbonate
Black shale
Multiple proxies
Microbial
Failed rift
Geothermal circulation

ABSTRACT

Toarcian black shale that hosts Mn-carbonate microbialites at Úrkút, Hungary was investigated by mineralogical, inorganic, and organic geochemical methods for characterization and comparison with other European black shales representative of the Toarcian Oceanic Anoxic Event. Based on the authigenic mineral composition, calculations were made to estimate environmental conditions during sediment accumulation and early diagenesis. Geochemical and petrographic results of organic, carbonate, and REE multiple-proxy analyses revealed a strong congruence between the host black shale and the Mn-carbonate ore beds. The Úrkút black shale is really a gray shale with moderate to low TOC contents that accumulated in a starved basin. The organic matter and anoxic characteristics resulted from rapid accumulation of organic matter from microbial booms, accompanied by a geothermally generated hydrothermal circulation system, and a high rate of authigenic mineral formation (clay minerals and proto-ore minerals). The inferred enzymatic Mn and Fe oxidation blocked carbonate formation by decreasing the pH. The system remained suboxic via syngenetic mineral accumulation (Fe-rich biomats), and became anoxic during diagenesis in conjunction with pyrite generation. The separation of black shale beds and Mn-ore beds is not distinct through the section. Instead, a distal hydrothermally induced clay-rich authigenic assemblage (marlstone) best describes the black shale, in which Mn-oxide proto-ore beds (Mn-rich laminae) formed from the beginning of black shale deposition, when the oxygen supply in the sedimentary basin was insufficient for enzymatic Mn(II) oxidation. Mn-oxide proto-ore was transformed to Mn-carbonate ore during microbially mediated processes during early diagenesis. The drivers for Mn-bearing organic matter-rich marlstones were most probably a combination of regional and local processes, with generation of a tectonic rift system that promoted geothermally generated hydrothermal fluids, which initiated microbial blooms. Black shale mineralogy, geochemistry, and organic matter at Úrkút differ from those of the epicontinental shelf black shales of the Tethyan Ocean.

1. Introduction

Organic geochemistry of black shales has been widely studied (e.g. Wignall, 1994; Jenkyns, 2010) because of their key role in understanding global changes, for example the Toarcian Ocean Anoxic Event (T-OAE). Black shales are of enormous economic importance because they are source rocks for the bulk of the World's hydrocarbons, and metalliferous black shales form ore deposits for many metals (e.g. Fe, Cu, Ni, Pb, V, Mo, Mn), and yet they are among the least understood sedimentary rock (e.g., Coveney and Chen, 1991;

* Corresponding author at: Research Center for Astronomy and Geosciences, Geobiomineralization and Astrobiological Research Group, Institute for Geology and Geochemistry, Hungarian Academy of Sciences, Budapest, Budaörsi str. 45, 1112 Budapest, Hungary.
E-mail addresses: rodokrozit@gmail.com (M. Polgári), jhein@usgs.gov (J.R. Hein), ls@gpi.uni-kiel.de (L. Schwark), palm@geo.u-szeged.hu (E. Pál-Molnár), manganvigh@vnet.hu (T. Vigh).

http://dx.doi.org/10.1016/j.palaeo.2016.06.030
0031-0182/

Pašava, 1993; Loukola-Ruskeeniemi, 1999; and others). The identification of paleo-oxygen levels is therefore of critical importance in the paleoenvironmental reconstruction and understanding the genesis of black shales (Wignall, 1994).

In the early Toarcian, global environmental change caused considerable mass extinction of terrestrial and marine organisms (Jenkyns, 1985, 1988; Pálfy and Smith, 2000; Pálfy et al., 2002). At the same time, a ~5–7‰ negative $\delta^{13}C$ excursion of carbon reservoirs was identified (marine organic matter, marine carbonate, terrestrial plants), as well as an abrupt increase of ocean water temperature (Küspert, 1982; Jenkyns and Clayton, 1997; Hesselbo et al., 2000; Rosales et al., 2004; Kemp et al., 2005). As a consequence of global, regional, and local effects, the accumulation of organic material increased resulting in a global distribution of black shales (Jenkyns, 1985, 1988; Haas, 2012).

For interpretation of the enriched organic matter accumulation and the negative $\delta^{13}C$ excursion, models were established. Among those models, some key global and local ones include: (i) Volcanism (Karoo–Ferrar continental plateau basalt formation) as a global catastrophe was the driving force for climate change that triggered black shale deposition. The global response to considerable volcanic CO_2 emission resulted in changes of sea level and current systems, which led to increased biomass productivity in upwelling zones (Jenkyns, 1985, 1988; Jenkyns and Clayton, 1997; Vető et al., 1997; Pálfy and Smith, 2000; Röhl et al., 2001; Schmid-Röhl et al., 2002; McArthur et al., 2008). (ii) Massive dissociation of methane hydrates caused by the warm climate was also proposed (Hesselbo et al., 2000; Kemp et al., 2005). (iii) Water stratification in silled basins may have obstructed oxygen supply, a local process without invoking global drivers (e.g., salinity differences, Röhl et al., 2001; Schmid-Röhl et al., 2002; Schwark and Frimmel, 2004; van de Schootbrugge et al., 2005). (iv) Mixed scenarios of global events, e.g. reduced levels of atmospheric oxygen and global ocean changes (Hallam, 1967, 1981). Early Toarcian black shales occur worldwide, although their onset and decline are potentially diachronous (Wignall et al., 2005). Understanding the conditions of formation and paleoenvironments of the black shales is important; clarification of global, regional, and local drivers is a great challenge (Haas, 2012).

Two types of lower Toarcian black shales of the western Tethyan Ocean can be distinguished (Jenkyns, 1985, 1988): (i) accumulation on an epicontinental shelf [(boreal, Jet Rock, Great Britain (Sælen et al., 2000); Schistes Cartons, Paris Basin, France (Hollander et al., 1991; Katz, 1994); Posidonia Shale, Germany (Röhl et al., 2001); Lusitanian Basin, Portugal (Jenkyns, 1985, 1988; Duarte, 1998)] and (ii) Alpine–Mediterranean Tethyan Region [(Umbria–Marche Basin, Italy (Jenkyns, 1985, 1988; Duarte, 1998); Úrkút basin, Hungary (Polgári, 1993; Vető et al., 1997; Polgári et al., 2012a)]. The boreal type occurs as shallow-water shelf sediments 15–30 m thick, with 5–15 wt.% TOC and a Hydrogen Index (HI) of 300–600 mg HC/g TOC. The Alpine Mediterranean type occurs in pelagic limestone, in rifted areas of Atlantic-type continental margins, with TOC between 1 and 3 wt.% (up to 10 wt.%), and a generally low HI, 200–300 mg HC/g TOC (Jenkyns, 1985, 1988). Transitional types exist, which show mixed features [(Mecsek Réka Valley Óbánya Siltstone Formation (MRV-ÓSF), Hungary (Varga et al., 2007; Raucsik and Varga, 2008a); Basque-Cantabrian Basin, northern Spain (Rosales et al., 2004)] (Fig. 1). Besides these typical Toarcian black shales, another classification differentiates between the pure non-ore bearing and an ore-bearing, namely Mn-carbonate types.

Sedimentary Mn deposits have a wide distribution in time and space (Roy, 1981). Their formation extends through more than half of geological history and they are extensively distributed both in the geological record on the continents and on the bottom of the present-day oceans, shallow seas, and lakes. The Jurassic (Toarcian) was an important time of Mn-carbonate mineralization and different ideas about the controls on deposit formation have been put forward, including tectonic activity, volcanism, climatic variations, and combinations of these. Mn-carbonate deposits are typically associated with organic carbon-rich beds (Roy, 1981). Black shale-hosted Mn-carbonate deposits are numerous and most deposits have large reserves of manganese ore with grades of 20–30 wt.% Mn. Numerous subeconomic black shale-hosted Mn deposits occur along with the giant Úrkút deposit in the Alpine–Mediterranean Tethyan Realm (Transdanubian Range: TR) (Jenkyns, 1988; Jenkyns et al., 1991). Stratiform black shale-hosted Mn-carbonate deposits reached maximum development during the Toarcian *tenuicostatum–falciferum* ammonite zones in the Strubberg and Allgäu deposits of the Northern Calcareous Alps and Eastern Alps, the Úrkút deposit in the TR of the Southern Alps, in the Tatra unit, and lower Carpathians (Polgári et al., 2012a and references therein).

At different locations, the black shale-Mn associations show similarities and differences: (1) contemporaneous oxic deposits formed under similar environmental conditions occur in some locations (Jenkyns, 1988); (2) not all black shale sections are enriched in manganese (Jenkyns, 1988; Jenkyns et al., 1991, 2001); (3) if they are Mn-rich, the TOC content is relatively low, only 4–5 wt.%, which may support a microbial origin for the Mn-carbonate deposits (Jenkyns, 1988; Polgári et al., 2012a); (4) negative $\delta^{13}C$ values of early diagenetic $MnCO_3$ support a contribution from organic carbon to the dissolved carbon reservoir (Polgári et al., 1991); (5) Mn(IV, III) oxides characterized the proto-ore because initial metal enrichment took place in an oxic seafloor environment (Polgári et al., 2012a). This oxic depositional environment contrasts with the generally accepted explanation for the formation of a laminated black shale, assumed to result from very limited benthic infauna. (6) High primary productivity occurred during black shale deposition (Jenkyns, 1988, 2010; Jenkyns et al., 1991, 2001; Vető et al., 1997) and biomarker studies indicate that organic matter in all these lower Toarcian black shales is dominantly of marine origin, derived from algal and bacterial sources (Farrimond et al., 1989; Polgári et al., 1992; Polgári, 1993; Jenkyns et al., 2001). (7) Formation of $MnCO_3$ immediately pre-dated deposition of the TOC-rich shales in the majority of localities suggesting that their deposition was characteristic of environmental conditions immediately preceding the anoxic event (Jenkyns et al., 1991). (8) Black shale formation was structurally confined to rifted continental margins of the developing Tethyan Ocean (Bernoulli and Jenkyns, 1974; Channell et al., 1992). Wignall (1994) stressed the possibility that abundant organic carbon deposition overwhelmed the benthos, thereby promoting formation of laminae even with oxic bottom waters.

Diagenetic processes overprinted the seabed manganese depositional signals and caused significant transformations, such as formation of early diagenetic rhodochrosite (e.g. Polgári et al., 1991). The large mass of bacteria living in and on the surface of the sediment provided a large pool of reactive organic matter after death that promoted a series of diagenetic reactions. During decomposition, the consumption of the organic matter by other microbial consortia may have played a key role in diagenesis through formation of the Mn-carbonate ore. Those anaerobic bacterial cycles were different from the syndepositional aerobic bacterial cycle, although both occurred contemporaneously at different depths in the sediment column (Polgári et al., 2012a).

The black shale-hosted stratiform Mn-carbonate deposits were reported to have mainly a hydrothermal metal source and microbial processes were thought to have occurred in some of the deposits (Cornelius and Plöchinger, 1952; Gruss, 1956; Polák, 1957; Andrusov, 1965; Germann and Waldvogel, 1971; Germann, 1971; Bernoulli and Jenkyns, 1974; Faupl et al., 1982; Beran et al., 1983; Jenkyns, 1988; Krainer et al., 1994; Krajewsky et al., 2001; Rantitsch et al., 2003; Polgári et al., 2012a,b). During the past 100 years, numerous studies have addressed the complex formation of the Jurassic black shale-hosted Mn-carbonate ore at Úrkút. The ore beds are now thought to have resulted from a two-step, microbially mediated process that produced a microbialite (Polgári et al., 2003a,b, 2012a,b, 2013a,b, 2016). This important deposit is among the 10 largest Mn deposits in its type with

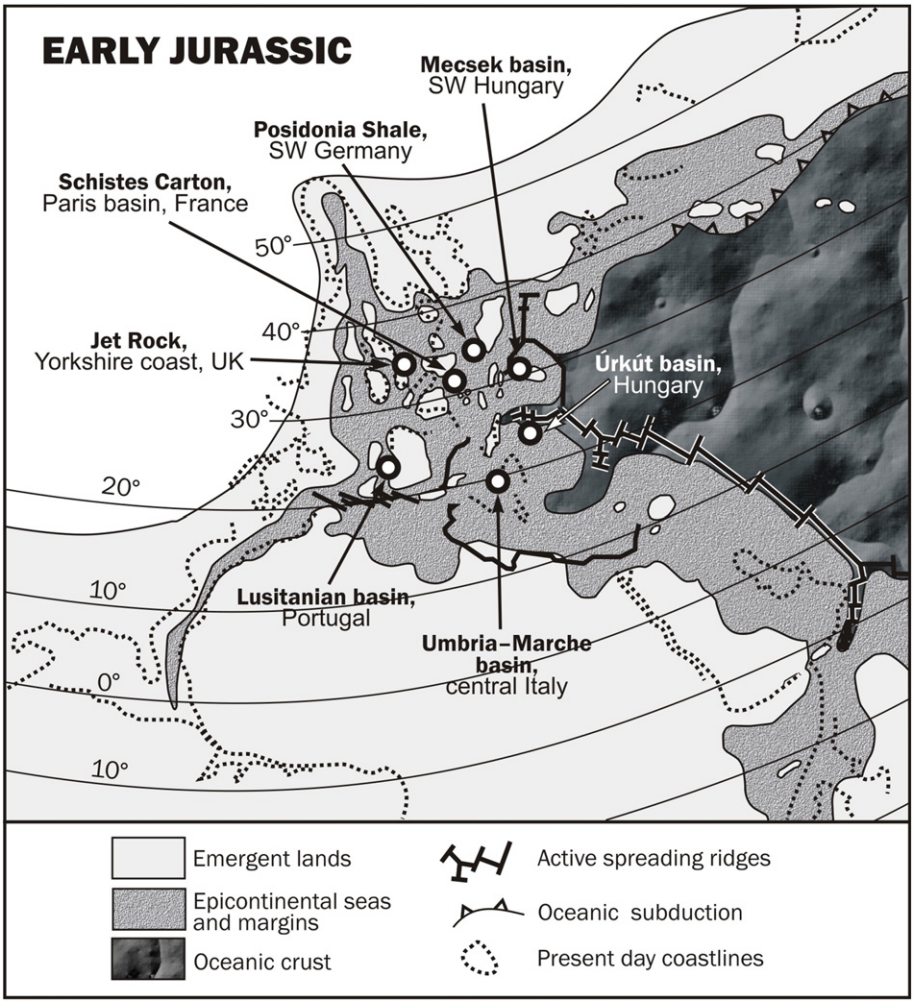

Fig. 1. Paleogeography of the Early Jurassic of Europe, after Bassoullet et al. (1993), with locations of some lower Toarcian black shale sections (Jenkyns, 1985, 1988; Duarte, 1998).

current reserves of 80 million tons of Mn-carbonate ore (24 wt.% average Mn and 10 wt.% Fe). The original deposit was much larger, a real giant, hosting about 300 million tons of ore, but much of it was eroded during the Cretaceous and Eocene (Szabó and Grasselly, 1980). The original features of the deposit were overprinted only by diagenesis, and have remained unaffected by significant thermal maturation. The ore deposit and its host black shale have been related to the T-OAE.

Application of models for understanding ancient Mn-carbonates hosted in black shale is difficult, even for unmetamorphosed deposits, because of overprinting of different microbially mediated early-diagenetic processes that took place. The effect is as yet unclear with respect to the role of the black shale host rock, the nature of the contained organic matter, the types of microbiota involved in the primary productivity and the nutrient cycle that supported it, and what microbiota were responsible for aiding the accumulation of huge quantities of metals. These are important questions not only from a scientific point of view but can also contribute to identifying guides for mineral deposit exploration. The age of the Úrkút black shale coincides with the T-OAE and comparison of this black shale to other Toarcian black shales and environments of formation is essential to addressing these questions.

The well-preserved, unmetamorphosed black shale that hosts Mn-carbonate deposits of the Úrkút basin (Fig. 2abc) offers an excellent case study for detailed petrographic, mineralogical, geochemical, and textural analyses. We completed mineralogical and chemical analysis, Rock-Eval pyrolysis, and stable isotope analysis to study basic inorganic and organic geochemical features (kerogen type, maturity, organic petrology). We compare the results with data available in the literature, focusing on the black shale from the lower part of the MRV-ÓSF Hungary (Varga et al., 2007) and former data from Úrkút (Polgári et al., 1991, 1992, 2000). We also include data from the Mn-ore sections (Vető et al., 1997).

This paper reviews the main characteristics of the black shale that hosts the Úrkút Mn deposit (Alpine–Mediterranean Tethyan Region), provides additional microtextural, mineralogical and geochemical evidence for the fundamental processes of its formation and its relation to the ore beds, discusses the importance of such deposits in developing paleoenvironmental indicators, provides a new general model for the origin of this type of black shale deposit, and discusses the importance of deposit characteristics for the interpretation of deposit genesis in the framework of the T-OAE.

2. Geological setting

The TR of Hungary is an important region for a series of Jurassic black shales and their associated Mn mineralization. The Úrkút black shale is located in the Bakony Mountains, which belong tectonically to the North Pannonian unit of the Alps–Carpathians–Pannonian regions (ALCAPA, Fig. 2ab). The largest Mn deposits occur in the Úrkút basin and at Eplény, which formed by the NW-SE trending block faulting that characterized the Late Triassic and Jurassic of this region (Fig. 2b). These deposits are within marine sedimentary rocks composed mainly

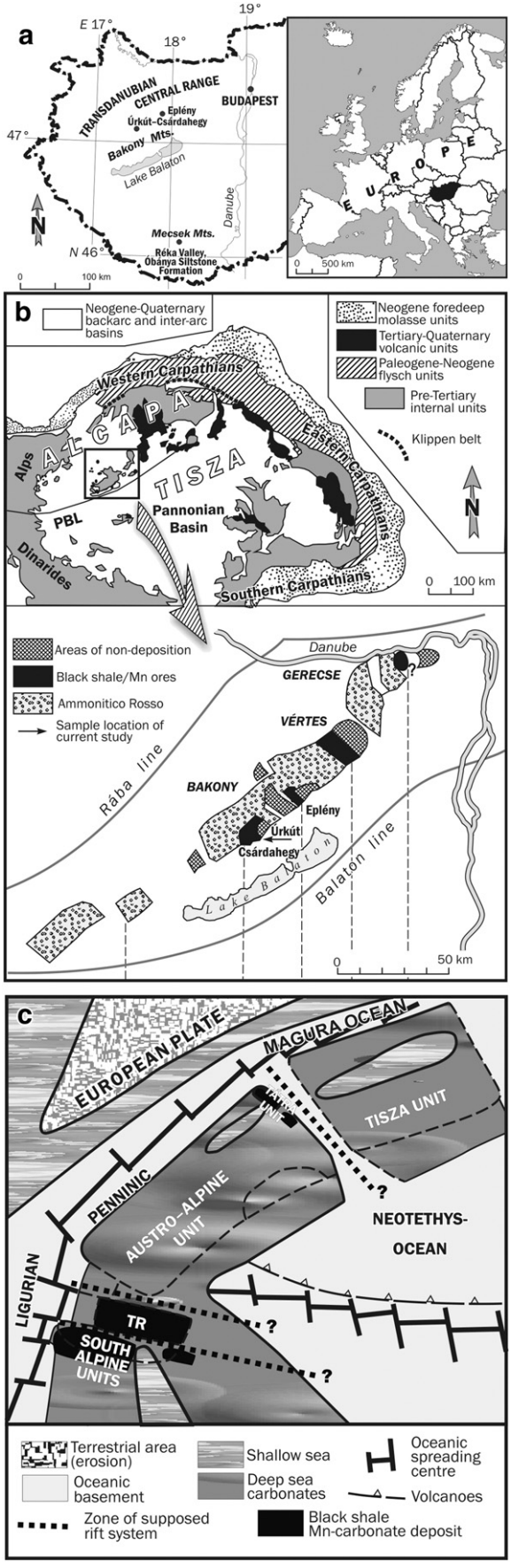

Fig. 2. Location of study area (a), Tectonic units and main formations of the Úrkút deposit (b), tectonic map of Jurassic Tethyan Realm (TR) (c) (modified after Polgári et al. (2012a)).

of bioclastic limestone, radiolarian marlstone, and dark-gray to black shale (Polgári, 1993).

The Úrkút Mn mineralization occurs in two main units in the 40 m thick section (Fig. 3, Supporting Information hereafter SI. 1). (1) Cherty, Fe-rich, Mn-oxide mineralization occurs in varicolored metalliferous claystones that overlie strongly leached limestone (Úrkút-Csárdahegy and Eplény, Polgári et al., 2012a). Currently, the extent of the ore deposit of economic importance is about 8 km^2.

The black shale (clayey marlstone)-hosted Mn mineralization (2) is Toarcian (*falciferum* ammonite zone; Géczy, 1973). The marlstone rests conformably on middle Lias carbonate rocks. Mn-ore mineralization is restricted to two main intervals within the marlstone, separated by black shale units (Bs1, Bs2, Bs3-4, Figs. 3, 4, SI. 2). The lower first (main) ore bed is about 8–12 m thick. The base of the first ore bed begins with 0.5 to 1 m thick black shale (Bs1), which is greenish, organic-rich, pyritiferous, containing enrichments of trace elements, Co, Ni, Cu in high As-bearing sulfides, and Sr-bearing barite (Polgári, 1993; Polgári et al., 2003a). The upper mineralized zone (second ore bed) is 2 to 4 m thick and is separated from the first ore bed by 10 to 25 m of black shale (Bs2). The second ore bed can interfinger with black shale (Bs3-4). The Ca-rhodochrosite ore is composed of alternating gray, green, brown, and black sections of finely laminated, very fine-grained clay mineral carbonate mixtures (Cseh Németh et al., 1980). Fine-grained (1–2 μm) rhodochrosite rock lacks coarse detritus and is laminated (Szabó-Drubina, 1959). Mineralized sections lack fossils including benthic trace fossils, and only rarely contain fish remnants as well as silicified, Mn-replaced, or coalified plant fragments (Polgári et al., 2005). The ore body formed in a structurally controlled marine basin via bacterial enrichment of Mn and bacterially mediated, early diagenetic formation of Mn carbonates. It has been proposed that hydrothermal fluids venting into the depositional basin were involved in the mineralization (Polgári et al., 2012a). The Fe and Mn oxides were probably deposited from deep-sourced fluids circulating through basement rocks. Circulation along zones of structural weakness was likely driven by high geothermal gradients (Polgári et al., 2004, 2007, 2012a).

The history of development of the Mesozoic TR in the ALCAPA was determined from its paleogeographic position in the Tethyan system. The Transdanubian terrane, part of the Tethyan shelf, was located between the Southern Alps and the Upper Austro-Alpine nappes during the complex development of the Mesozoic ocean (Fig. 2c). Its initial displacement started during the Eocene by way of NE lateral motion and it arrived at its present location in the early Miocene (Kázmér and Kovács, 1985; Csontos and Vörös, 2004). A Middle Jurassic paleogeographic map (Haas, 1994) shows that the input of terrestrial detritus was blocked by the Ligur-Pennine Ocean and the Neotethys (Fig. 2c). Continental volcanic activity and oceanic spreading centers were widespread in the Neotethys and Ligurian–Penninic Oceans.

3. Samples and methods

Oriented samples from bottom to top (n = 19) were collected through the entire black shale sections hosting the Mn-ore beds (Table 1, SI. 1). Besides the new collection (n = 19, FP series, Fig. 3), previously collected samples were also taken into consideration (n = 12) (Polgári et al., 2012a, 2016). Bulk and individual lamina sub-samples were examined to determine macroscopic features (FP series Fig. 4, SI 2). FP3–FP11 are not oriented samples. Petrographic structural–textural studies were made on 14 oriented thin sections in transmitted light (NIKON ECLIPSE 600 rock microscope, IGG, HAS, Budapest).

X-ray powder diffraction of 44 samples including subsamples for mineralogy was done using a Philips X-ray diffractometer (PW 1710) with carbon monochromator and Cu Kα radiation. Mineral composition was determined on randomly oriented powdered samples by semi-quantitative phase analysis according to the modified method of Bárdossy et al. (1980), using previously defined intensity factors.

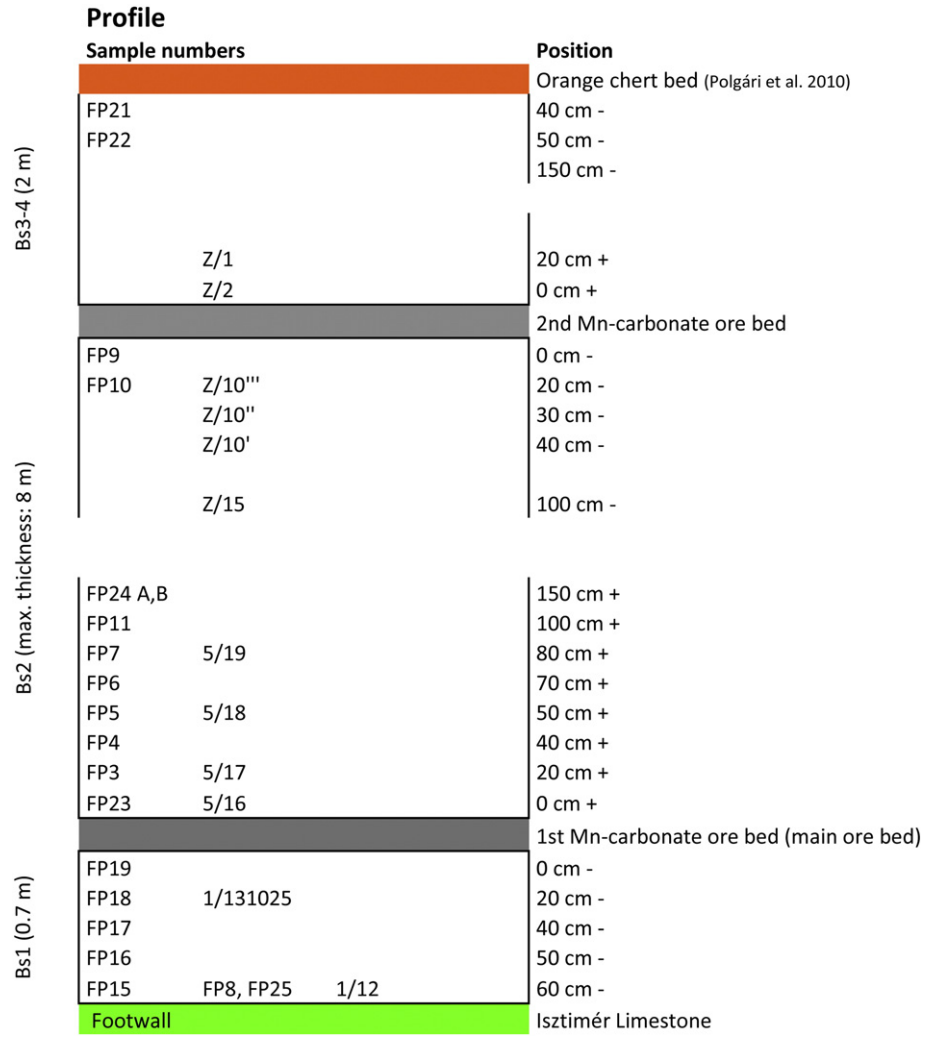

Fig. 3. Profile of black shale host of Mn-carbonate deposit and location of samples; this is a composite log without ore beds, so the thickness of the ore beds and chert-ironstone are not to scale; the − after cm means below the Mn-carbonate ore beds and the + means above the Mn-carbonate ore beds; Úrkút mine, Shaft No. III, western minefield, +186 mBf; Bs = black shale (Collected by T. Vigh, Mangán Ltd. Úrkút).

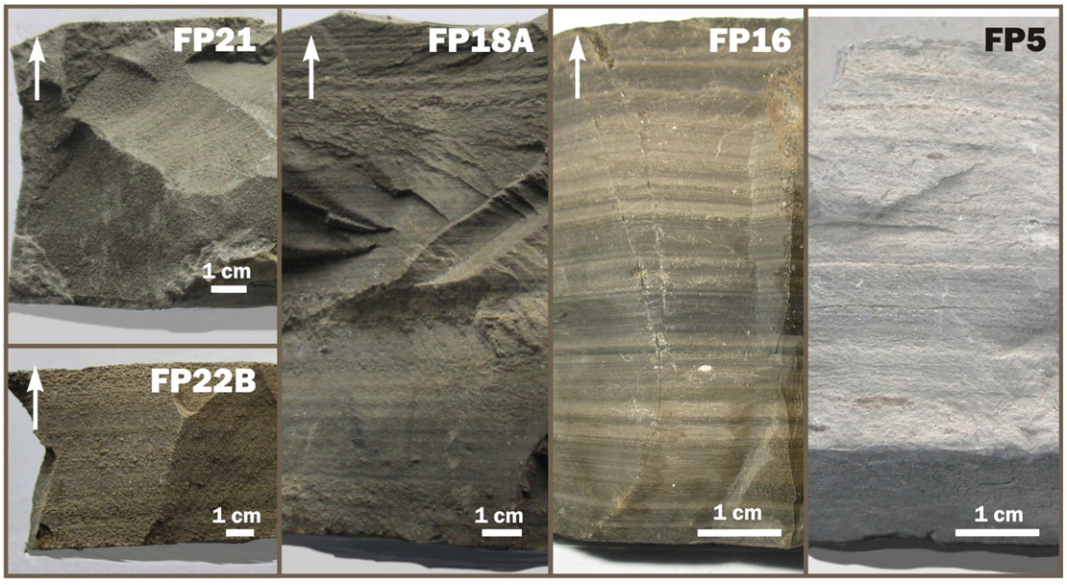

Fig. 4. Representative samples. Arrow shows up direction; no arrow means not oriented. (Photos by M. Polgári).

Table 1
List of samples and used methods (Úrkút mine, Shaft No. III, western minefield, +186 mBf).

No.	Samples	Subsamples	Bs zone	Methods						
				A	B	C	D	E	F	G
1	FP3*		Bs2	X		X	X	X		X
2	FP4		Bs2	X		X	X	X		X
3	FP5		Bs2	X	X	X	X	X		X
4	FP6		Bs2	X		X	X	X		X
5	FP7		Bs2	X	X	X	X	X		X
6	FP8		Bs1	X		X	X	X		X
7	FP9		Bs2	X	X	X	X	X		X
8	FP10		Bs2	X	X	X	X	X		X
9	FP11		Bs2	X		X	X	X		X
10	FP15		Bs1	X		X	X	X		X
11	FP16		Bs1	X	X	X				X
12		FP16A	Bs1	X		X	X	X	X	X
13		FP16B	Bs1	X		X	X	X		X
14	FP17		Bs1	X	X	X	X	X		X
15	FP18		Bs1	X		X				
16		FP18A	Bs1				X	X		X
17		FP18B	Bs1				X	X		X
18	FP19		Bs1	X		X	X	X		X
19	FP21		Bs3-4	X		X	X	X		X
20	FP22		Bs3-4	X		X				
21		FP22A	Bs3-4			X	X	X	X	X
22		FP22B	Bs3-4			X	X	X		X
23		FP22C	Bs3-4			X	X	X		X
24		FP22D	Bs3-4			X	X	X		X
25	FP23		Bs2	X	X	X				
26		FP23A	Bs2	X		X	X	X		X
27		FP23B1	Bs2	X		X	X	X		X
28		FP23B2	Bs2	X		X	X	X		X
29	FP24		Bs2	X	X	X				
30		FP24A	Bs2	X		X	X	X		X
31		FP24B	Bs2	X		X	X	X		X
32	FP25		Bs2	X		X				
33		FP25A	Bs2	X		X	X	X		X
34		FP25B	Bs2	X		X	X	X		X
35	1/131025**		Bs1	X		X				
36	1/12		Bs1	X		X				
37	5/16		Bs2	X		X				
38	5/17		Bs2	X		X	X	X		
39	5/18		Bs2	X		X	X	X		
40	5/19		Bs2	X		X	X	X		
41	Z/1		Bs3-4	X		X	X	X		
42	Z/2		Bs3-4	X		X	X	X		
43	Z/10'		Bs2	X		X	X	X		
44	Z/10"		Bs2	X		X	X	X		
45	Z/10"'		Bs2	X		X	X	X		
46	Z/15		Bs2	X		X	X	X		

Legend: *: Samples 1–9 are not oriented; samples 10–46 are oriented from bottom to top.
**: Samples 35–46 are from Polgári et al. (2012a, 2016).
A — rock microscopy; B — UV microscopy for maceral analyses; C – X-ray powder diffraction (XRD); D – Mass spectrometry (MS); E – Gas-chromatography mass spectroscopy (GC—MS); F — Fourier transform infrared spectroscopy (FTIR); G — Chemical analysis (ICP, XRF, MP-AES).
The archive samples can be found at the storage of Institute for Geological and Geochemical Research, HAS.

Black shale samples were analyzed for chemical and mineralogical contents (n = 29, sub-samples were the following: FP16, FP16A, FP16B (A-lower part; B-upper part of samples, B1-lower part; B2-upper part of samples), FP23A, FP23B1, FP23B2, FP25AB). The samples were analyzed for 40 major, minor, and trace elements using XRF method for main elements (Si, Ti, Al, Fe, Mn, Mg, Ca, Na, K and P), and using 4-acid digestion (hydrochloric, hydrofluoric, nitric, perchloric acids) in conjunction with inductively coupled plasma-atomic emission spectrometry (ICP-AES; minor and trace elements) and ICP-mass spectrometry (ICP-MS, rare earth elements-REE) SGS Laboratories, Ottawa, Canada. The resulting solutions were taken to dryness and the residue dissolved with 1 ml of aqua regia and then diluted to 10.0 g with 1% (volume/volume) nitric acid. Another split of each sample was fused with lithium metaborate then analyzed by X-ray fluorescence after acid dissolution of the fusion disk. This technique, provides analysis of all major elements, including Si, and a few minor and trace elements. The accuracy of Si determinations was good, about 2–4% based on the total-oxide sums, even for high-Si chert. Sr and Ba contents were determined by both the 4-acid digestion and fused disc techniques, which produced comparable results. Titanium and Cr were also analyzed using both techniques, but only data from the fused-disc technique are used because the fusion technique more completely digests refractory minerals that might contain those elements.

Se, Te, As, Sb, and Tl concentrations were determined using hydride generation followed by atomic absorption spectrometry (AAS). Mercury was determined by cold vapor AAS.

Preliminary information of the major contributors to OM content were determined by Rock-Eval analysis (n = 27). Rock-Eval measurements were carried out at the University of Kiel, Germany using VINCI Rock Eval II Plus instrument following established protocols (Espitalié et al., 1985).

Maceral analysis at reflected white light and excited blue light observations supported the organic matter studies on ground whole-rock samples embedded in epoxy resin and polished according to ISO7404-2 standard. Maceral analysis and vitrinite reflectance measurements followed the method of Taylor et al. (1998). Here, the main ore bed and the overlying black shale Bs2 zones were sampled and analyzed using 14 samples. Maceral analysis was carried out not only on marly shales but also five green and brownish gray finely laminated Mn-carbonate samples from the main ore bed.

Organic carbon isotopic compositions were measured, after decarbonation, using a Finnigan Delta V continuous-flow mass spectrometer equipped with a Thermo Flash elemental analyzer (IGG, HAS, Budapest) (n = 29). Standard deviation of the data is below 0.1‰ based on the reproducibility of sample and laboratory standard data. $\delta^{13}C_{VPDB}$ and $\delta^{18}O_{SMOW}$ data were measured for carbonates (n = 27).

Fourier Transformed Infra Red spectroscopy (FTIR) measurements were done using a Bruker VERTEX 70 Fourier transform infrared spectrometer equipped with a Bruker Hyperion 2000 microscope with 20× ATR objective and MCT-A detector (IGG, HAS, Budapest) (Two representative samples were studied, FP16A and FP22A). During ATR analysis, samples were contacted with the tip of the Ge crystal (0.5 μm) on 1 N pressure. The measurements were conducted for 32 s in the 600–4000 cm^{-1} range with 4 cm^{-1} resolution. Opus 5.5 software was used to evaluate the data. Contamination of epoxy glue and glass was taken into consideration, and peaks of these phases were not considered.

4. Results

4.1. Bulk mineralogy (XRD)

The black shale minerals are typically microcrystalline, averaging 1–2 μm in size, with very rare detrital mineral grains up to several tens of micrometers in diameter (e.g. quartz, feldspar). Black shale mineralogy and mineral genesis, grouped by mineral types, are summarized in Table 2. The mineral distribution varies among and within each of the black shale sections (Fig. 5). The mineral assemblage is similar to that of the ore beds, but they occur in different proportions. The bulk mineralogy of the Mn-carbonate ore beds is dominated by rhodochrosite (Ca-, Mg-bearing), siderite (second bed), kutnohorite, celadonite, nontronite, goethite, quartz, Ca-apatite (phosphorite), and pyrite, with traces of chlorite, zeolite, feldspar, and manganite (Polgári et al., 2012a). The bulk mineralogical composition of the black shale consists of (i) carbonates (calcite, dolomite, rhodochrosite, kutnohorite, siderite); (ii) oxides (quartz); (iii) silicates/clays (smectite, celadonite, chlorite, kaolinite), K-feldspar, plagioclase and zeolite; (iv) sulfides (pyrite); (v) and sulfates (gypsum, barite).

The black shale is dominated by authigenic clay minerals such as smectite and celadonite, as well as quartz, but in some sections the

Table 2
Black shale mineralogy and mineral genesis, grouped by mineral types based on XRD, rock microscopy and IR.

Minerals grouped on genetic aspects											
Mineral group	Minerals	Authigenic		Biodebris*	Terrigenous	Diagenetic (from authigenic)		Authigenic not affected by diagenesis	Diagenetic (from terrigenous)		Terrigenous not affected by diagenesis	Secondary alteration
		Microbially mediated (mm)	Non-mm			Microbially mediated (mm)	Non-mm		Microbially mediated (mm)	Non-mm		
Carbonates	Calcite			*								
	Dolomite					*					*	
	Rhodochrosite					*						
	Kutnohorite						*					
	Siderite					*						
Oxides	Quartz	*?	*	*	* (wind blown)	*?	*	*			*	
	Goethite	*				*						
Phyllosilicates	Smectite	*						*				
	Celadonite	*						*				
	Chlorite, kaolinite (clay)				*						*	
Tectosilicates	K-feldspar				* (volcanic ash)						*	
	Plagioclase				* (volcanic ash)						*	
	Zeolite (clinoptilolite)									* (tuff alteration, algae-filling)		
Sulfides	Pyrite					*	*					
Sulfates	Gypsum											*
	Barite						*					
Phosphates	Apatite			*								

* biodebris is not affected by diagenesis

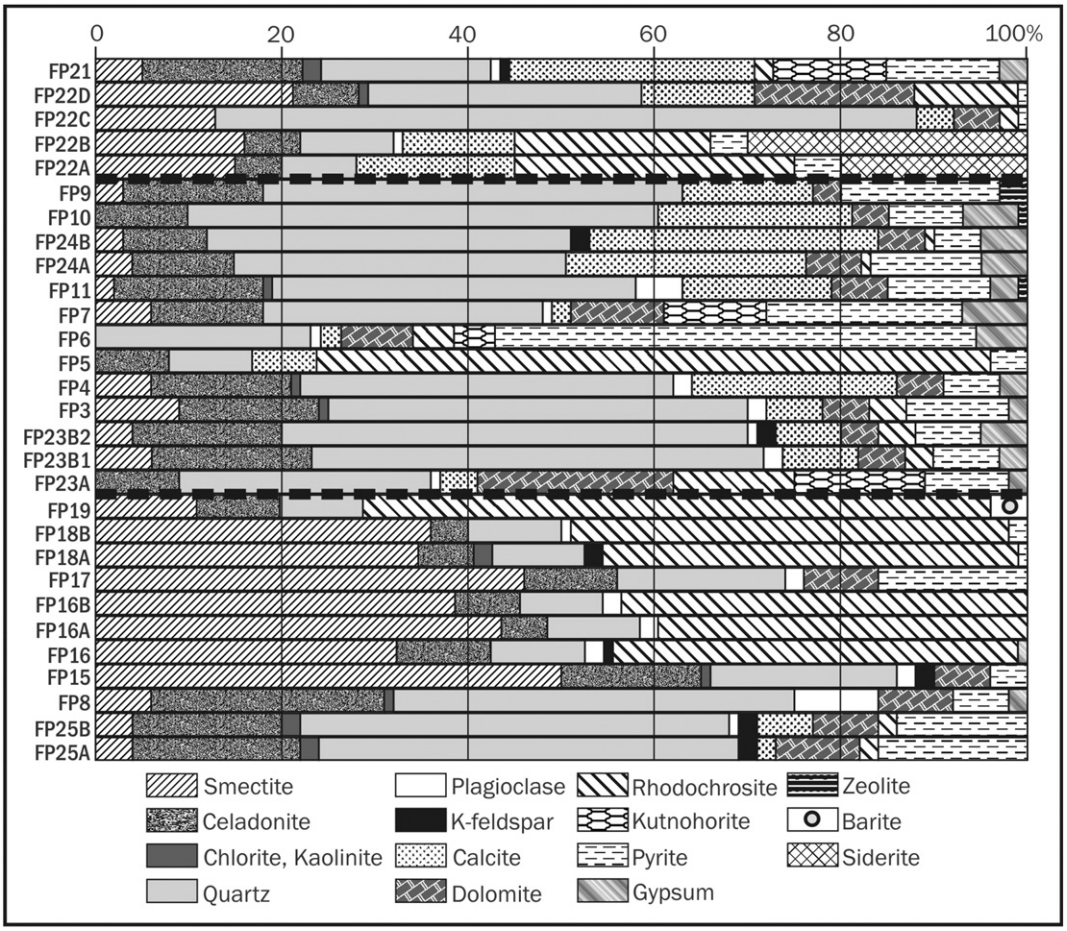

Fig. 5. XRD mineralogy. The bold dashed lines represent ore beds.

content of dolomite, K-feldspar, and plagioclase increses moderately. Calcite is also enriched in some laminae. Rhodochrosite-rich laminae first occur very close (few cm) to the contact zone of the footwall in the black shale Bs1 (Fig. 5). Pyrite occurs commonly in the black shale sections. The second ore bed is characterized by alternating thin ore and black shale layers, which are macroscopically not distinguisable. Other minerals occur as trace components.

4.2. Rock microscopy

Thin sections show a representative series of partly pyritized Fe-rich biomats occurring as brown goethitic finely woven microtextures in a fine-grained matrix (Fig. 6a–h, SI. 3). This typical texture occurs from the bottom to the top of the sections. Fish debris composed of apatite is very common in the samples (Fig. 6dh). Carbonate biodebris and other mineral clasts (quartz) are enriched in distinct intervals, or occur randomly. The fine-grained matrix is carbonate-bearing and clay-mineral rich.

4.3. Fourier Transformed Infra Red spectroscopy (FTIR)

Verification of goethite and apatite was made by FTIR from thin sections (Table 2).

FP16A and FP22A samples both contain iron oxides with clay minerals and carbonates (SI. 4). The IR spectra were taken on fine-grained patches with reddish-brown material in transmitted light. The iron oxides were determined after Glotch and Rossman (2009). The IR spectra of FP16A and FP22A contain the Fe–O vibration of akaganéite (665 cm^{-1}), goethite (667 cm^{-1}, 805 cm^{-1}), and maghemite (730 cm^{-1}).

The characteristic infrared vibrations of clay minerals were identified after Madejová and Komadel (2001). Sample FP16A contains a mixture of kaolinite and smectite with peaks at 680 cm^{-1} (Si–O perpendicular stretching), 846 cm^{-1} (AlMgOH deformation), 1005 cm^{-1} (in-plane Si–O stretching), 3637 cm^{-1} (OH stretching of structural hydroxy groups), and 3734 (Si–OH bending of adsorbed water). Sample FP22A contains mostly smectite with characteristic peaks at 688 cm^{-1}, 841 cm^{-1}, 1011 cm^{-1}, 3573 cm^{-1} (bending of structural OH groups), and 3623 cm^{-1}.

The infrared molecular vibrations for carbonate were interpreted after Müller et al. (2014), which occur in both FP16A and FP22A samples. The FP16A has CO_3 peaks at 864 cm^{-1} and 1397 cm^{-1}, the C–O vibrations at 2343 and 2365 cm^{-1}. Sample FP22A contains only CO_3 bands of carbonate at 864 cm^{-1} and 1400 cm^{-1}. Organic material and hydroxyapatite were identified only in sample FP22A.

The organic material was identified after Parikh and Chorover (2006). The band at 1526 cm^{-1} is attributed to C–N and C–H deformation, the band at 1705 cm^{-1} to C–O and C–H vibrations. Both of the above-mentioned peaks are characteristic for amides.

The infrared peaks of apatite were identified following Figueiredo et al. (2012), with structural PO_4 vibrations at 872 cm^{-1} and 1012 cm^{-1}.

4.4. Chemistry

Chemical compositions are summarized in SI., 5, and 6, and based on those data, paleoenvironmental proxies were calculated based on Al-normalized values (Table 3A).

The Úrkút black shale has average contents of 18.2 wt.% Si (max: 27.0%), 3.7 wt.% Al (max: 6.2%), 6.9 wt.% Fe (max: 17.3%), 5.7 wt.% Mn (max: 20.9%), and 5.3 wt.% Ca (max: 10.6%). The concentration of S is 2.0 wt.% on average (max: 4.5%), which reflects the high pyrite content of the black shale. Other components on average are below 1 wt.%, but the maximum P content reaches 2.8 wt.%.

Enrichment factors (EF) of elements in the black shales compared to Average Shale (Wedepohl, 1971) show a mean for Mn of 7.2, Fe of 2.5, and P of 3.7, while the mean S content shows a high EF (11.7). V (average 100 ppm, max. 183 ppm), Mo (average 7.9 ppm max. 15 ppm), and Cr are depleted in the black shale relative to average shale. Ni is near crustal abundance, although Cu has an EF in the Úrkút black shale of 3.

4.5. Organic geochemistry and petrology

Total organic carbon (TOC) values in Bs1 range between 0.59 wt.% and 1.06 wt.% (mean 0.84%), in Bs2 between 0.56 wt.% and 3.53 wt.% (mean 2.08%), and in Bs3-4 between 0.61 wt.% and 1.73 wt.% (mean 1.12%) (Table 4). TOC correlates with N content reflecting the organic origin of N. C/N ratios scatter around 20, and in Bs1 it ranges between 14 and 21 (with one outlier value of 31.5), in Bs2 C/N ratios range between 14 and 27, and in Bs3-4 between 17 and 23, showing relatively higher values in Bs2. Carbon isotopic composition of organic matter in Bs1 varies from –30.5‰ to –33.6‰ (VPDB), in Bs2 from –31.8‰ to –32.9‰ (VPDB), and in Bs3-4 from –29.9‰ to –30.8‰ (VPDB). Bs2 shows less negative carbonate $\delta^{13}C$ (–2.8‰ to –18.1‰ VPDB) and more negative $\delta^{18}O$ values (–1.7‰ to –4.1‰ SMOW) compared to Bs1 ($\delta^{13}C$ –5.1‰ to –9.8‰ VPDB); $\delta^{18}O$ +0.9‰ to –1.8‰ SMOW) and Bs3-4 ($\delta^{13}C$ –4.0‰ to –10.0‰ VPDB); $\delta^{18}O$ –0.6‰ to –2.8‰ SMOW). Hydrogen Index (HI) values indicate algal contributions (Type-II kerogen) in Bs2, while Bs1 and Bs3-4 samples are characterized by values representative of oxidized organic matter or Type-III kerogen. HI and its correlation with TOC values are generally higher in Bs2 (87–490 mg HC/g TOC) than in the other sections (41–106 and 55–172 mg HC/g TOC for Bs1 and Bs3-4, respectively). The values in the second ore bed are not lower than in Bs1 and Bs3-4. The $\delta^{13}C$ values of organic matter (OM) show a tendency towards less negative values up through the entire section, and a slight positive shift in the first ore bed (main ore bed).

S1 values are below 0.5 mg CH/g of rock in all samples, while S2 values above 5 mg CH/g of rock (good CH potential) are only found in the upper part of Bs2, and fall below 5, generally below 2.5 in other parts of the section (fair and poor source rock, respectively). T_{max} is below 435 °C in all black shale sections and does not show stratigraphic trends. All the samples are in the early stage of diagenesis.

TOC, N, C/N, S1, S2, and HI values show an increasing trend towards the inner parts (between 12.25 and 17.70 m) of Bs2. That depth interval could not be sampled in the mine due to the lack of access. However, the inclusion of data from Vető et al. (1997; see Discussion) documents the lack of trends through that interval.

The average vitrinite reflectance is 0.3%. The black shale samples are generally rich in liptinite, where weak brownish fluorescing and non-fluorescing bituminite and liptodetrinite of solitary alga are the major constituents, 45–95% of the OM (SI. 7). The occurrence of vitrinite and inertinite of terrestrial origin is subordinant through the entire profile. The occurrence of 5 μm size vitrinite particles is the highest in the main ore bed that ranges from 5% to 50% in relative volume from the lower 0.85 m to 3 m distance from the underlying limestone. The size of vitrinite particles increases in the Bs2 to 50–100 μm at the top and their relative contribution to the OM decreases in the middle part of the unit because liptinites became more abundant there in accord with the TOC and elevated HI. Inertinite content is usually below 5% with the exception of the lowest sample of the main ore bed. Primary, morphologically recognizable 1–3 μm liptinites are represented by telalginite, tasmanites type alginite and liptodetrinite of planktonic origin found through the entire section. Laminated alginite makes up 10–12% of the alginite but due to intense degradation their longer diameter is often limited to 20–50 μm. Telalginites most likely are the highest in the ore layers compared to the Bs2. This may be due to the higher resistance of exin cell walls to bacterial decomposition, and to the in situ oxidation during mineralization and precipitation of Mn and Fe with the consumption of the less resistant bituminite, laminated alginite, and liptodetrinite.

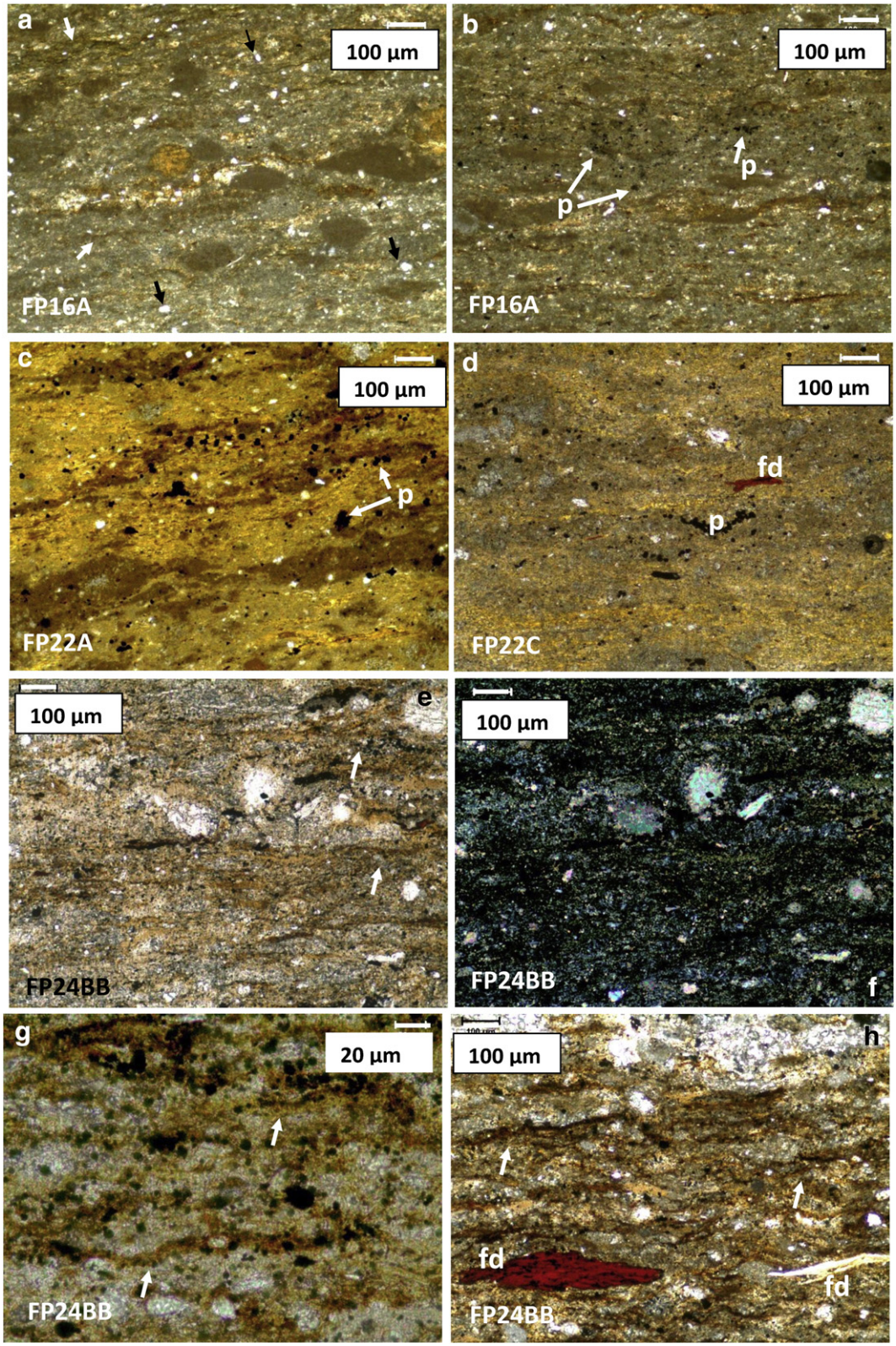

Fig. 6. Representative series of photomicrographs of partly pyritized Fe-rich biomats, petrographic microscope, transmitted light. (a) Sample FP16A series of Fe-rich biomats (white arrows) and detrital and biogenic debris (black arrows) in fine-grained matrix material (b) Pyritized Fe-rich biomats (p-pyrite); (c) FP22A pyritized Fe-rich biomats (p-pyrite); (d) FP22C series of partly pyritized (p) Fe-rich biomats and fish debris (fd, apatite); (e) FP24BB series of partly pyritized (arrows) Fe-rich biomats; (f) Crossed Nicol of (e); (g) Series of partly pyritized Fe-rich biomats (arrows); (h) Series of partly pyritized Fe-rich biomats (arrows) with fish debris (fp) and other detritus. For further details see Fig. 3 and SI 1, 2. (Photos by M. Polgári and I. Gyollai).

The bituminite content is the highest in the black shale with flaser texture recognized at 500 times magnification. Non-fluorescing bituminite is subordinant in the main ore bed, but its structure and appearance is similar to that observed in the Bs2-like biomats. The texture of the samples of the main ore bed shows similarities to the Bs2 samples.

Table 3
Comparison of chemical paleoenvironmental proxies of the black shale and Mn carbonate ore of Úrkút and Posidonia Shale.

Proxy	Black shale (Úrkút)	Mn carbonate ore (Úrkút)	Method	References
A				
Redox	Oxic	Oxic	U/Th	Yang et al. (2011)
Productivity	Moderate. At one-one sample: footwall, bed No. 2	Important in middle of main ore bed, moderate in bed No. 2	$Y^* = (Y/Al_2O_3)_{sample}$ ´ $(Al_2O_3)_{Upper\ Continental\ Crust}$ Y^*: Si, P, Ba	Schmitz et al. (1996)
Enrichment factor (EF median)	Te, **Co**, S, **As**, **Mn**, **Mo**, **Ca** > 5	**Co**, **Mn**, P, **Ca**, **Mo**, Ce, Ga, **As**, Sr > 5	EF(element) = $(element/Al)_{sapmle}$/ $(element/Al)_{Average\ Shale}$	Wedepohl (1971)
	REE 2.3	***REE ~ 4.3***		
	In, Hf, **K**, Ba, **Na** < 1	**K**, Rb, **Na** < 1		
	Max.: Co 15.0; (Te 17.4)	Max.: Co 37.9; Mn 34.6		
Element excess (Xs median)	Te, **Co**, S, **As**, **Mn**, **Mo**, **Ca**, **P**, Ag > 70%	**Co**, **Mn**, **P**, **Ca**, **Mo**, Ce, Ga, **As**, Sr, Fe, Mg, RFF, Ni, Y > 70%	Ex(element) = element – Al_{sample} $(element/Al)_{Average\ Shale}$	Brumsack (2006)
	REE: 56%	***REE: 76%***		
	Na, Ba, K, Hf, In, Rb, Bi <0%	Na, Rb, K <0%		
	Max.: Te, Co (93–94%)	Max.: Co, Mn (97%)		
Anomalies				
Pr	0.8	0.8	$Pr/Pr^* = 2\ Pr_{PAAS}/(Ce_{PAAS} + Nd_{PAAS})$	Bau and Dulski (1996)
Ce	1.42 (max. 1.51 main ore bed) cannot accept because of anomaly of Pr	1.35 (max. 2.12 main ore bed) cannot accept because of anomaly of Pr	$Ce_{anom} = Ce_{PAAS}/(2\ Pr_{PAAS}$ - $Nd_{PAAS})$	Bolhar et al. (2004)
La	0.90 cannot accept because of anomaly of Pr	0.88 cannot accept because of anomaly of Pr	$La_{anom} = La_{PAAS}/(3\ Pr_{PAAS} - 2\ Nd_{PAAS})$	Bolhar et al. (2004)
Eu	1.13 (max. 1.21 bed No. 2)	1.08 (max. 1.18 footwall + main ore bed + bed No. 2)	$Eu_{anom} = Eu_{PAAS}/(2/3\ Sm_{PAAS} + 1/3\ Tb_{PAAS})$	Bau and Dulski (1996)
Gd	1.10 normal marine	1.11 normal marine	$Gd_{anom} = Gd_{PAAS}/[(0.33\ Sm_{PAAS}) + (0.67\ Tb_{PAAS})]$	Bau et al. (1996)
Y	0.82 (decreases upward, more intense adsorption)	1.00 (low: footwall, main ore bed + decreases upward in bed No. 2)	$Y_{anom} = 2\ Y_{PAAS}/(Dy_{PAAS} + Ho_{PAAS})$	Bau et al. (1996)
ΔSm_{PAAS}	1.23 (decreases upward: decrease of MREE enrichment)	1.06 (high: footwall, main ore bed + top of bed No. 2)	$\Delta Sm_{PAAS} = Sm$ - (8 La_{PAAS} - 5 Yb_{PAAS})/13	Bright et al. (2009)
$(Nd/Yb)_{PAAS}$ (***LRFF/HRFF***)	1.11 (decreases upward: decrease of LREE enrichment)	1.27 (decreases upward: decrease of LREE enrichment)		Nothdruft et al. (2004)
$(Pr/Sm)_{PAAS}$ (***LRFF/MRFF***)	075 (decreases upward: decrease of LREE enrichment)	0.77 (intense decreases upward: decrease of LREE enrichment)		Nothdruft et al. (2004)
$(Sm/Yb)_{PAAS}$ (***MRFF/HRFF***)	1.45 (increases upward: increase of LREE enrichment)	1.55 (slightly increases upward: increase of LREE enrichment)		Nothdruft et al. (2004)
La vs. Ce	3.36 (increases upward: enrichment of Ce --> biogenic, terrigenous)	3.27 (increases upward: enrichment of Ce --> biogenic, terrigenous)		Toth (1980)
Y/Ho	22.29 (decreases upward: terrigenous effect, increase of adsorption)	29.31 (decreases upward: terrigenous effect, increase of adsorption)		Song et al. (2012)
Y/Ho vs. La	Terrigenous effect exist	Terrigenous effect exist		Song et al. (2012)
$(La/Yb)_{PAAS}$ vs. $(La/Sm)_{PAAS}$	Via early diagenesis: adsorption	Via early diagenesis: adsorption		Bau and Dulski (1996)
Sm/Yb vs. Eu/Sm, Y/Ho vs. Eu/Sm, Y/Ho vs. Sm/Yb	No direct hydrothermal effect	No direct hydrothermal effect		Bau and Dulski (1996)
Zr/Rb	Near 1 - fine grained sediments without Q input	1.32		Dypvik and Hams (2001)
Rb/Cs	15 ± 4 - fine grained sediments	16.74		Scheffler (2004)
Zr/Ti	0.03 - neutral magmatic rocks provenance area	0.03		Scheffler (2004)
Rb/K	0.002-0.003: fresh water input	0.003		Campbell and Williams (1965)
Co/Cr, Ni/Co, Co/Ni, U/Th V/Cr	Oxygenic conditions	Oxygenic conditions		Algeo and Maynard (2004)
V/(V + Ni)	Suboxic conditions (microbial mediation!)	Suboxic		Algeo and Maynard (2004)
(Cu + Mo)/Zn	Suboxic condition (microbial mediation!)	Suboxic condition (microbial mediation!)		Algeo and Maynard (2004)
CIA	≤50 fresh, not weathered, FP17-FP25A: CIA 50-60 slight weathering rate	<50		Nesbitt and Young (1982)

B	Black shale (Úrkút)	Posidonia Shale	João et al. (2012)
Proxy			
Enrichment factor (EF median)	Te, Co, S, As, Mn, Mo, Ca >5	S, Sc >5	
	In, Hf, K, Ba, Na <1	Sb, Rb, Ba, Ti, Zr, Mg, K, Na, Mn <1	
	Max.: Co 15.0; (Te 17.4)	Max: S 11.5	
Paleoredox			
Ni/Co	Oxic	Oxic	
V/Cr	Oxic-suboxic	Oxic	
V/(V + Ni)	Suboxic	Anoxic	
$Mn^* = log[(Mn/Mn_{PAAS})/(Fe/Fe_{PAAS})]$	Oxic-suboxic	Sub-anoxic	

Table 4
Organic geochemical and isotopic data.

Sample ID		Elevation	TOC	N	C	C/N	S1	S2	HI	T_{max}	$\delta^{13}C_{carb}$	$\delta^{18}O_{carb}$	$\delta^{13}C_{org}$
		(m)	(wt.%)	(wt.%)	(wt.%)		(mgCH/g rock)	(mgCH/g rock)	(mgCH/g TOC)	(°C)	‰ V-PDB	‰ V-SMOW	‰ V-PDB
FP21	Bs3-4	25.2	1.73	0.08	5.79	22.0	0.11	2.98	172	423	−4.0	−2.6	−30.6
FP22D		24.3	0.85	0.05	4.76	17.3	0.05	0.75	88	426	−9.1	−1.3	−30.8
FP22C		24.2	0.61	0.03	2.23	22.9	0.04	0.43	69	423	−7.7	−2.8	−29.9
FP22B		24.2	1.07	0.05	7.05	22.7	0.06	0.63	59	428	−9.4	−0.6	−30.7
FP22A		24.2	1.27	0.06	6.92	23.0	0.05	0.70	55	427	−10.0	−0.8	−30.8
Z/1		23.9	1.06	0.05	4.90	20.2	0.10	1.37	128	425	−8.1	−1.9	–
Z/2		23.7	1.24	0.06	5.90	20.1	0.08	1.59	129	422	−8.1	−1.4	–
Min			0.61	0.03	2.23	17.3	0.04	0.43	55	422	−10.0	−2.8	−30.8
Max			1.73	0.08	7.05	23.0	0.11	2.98	172	428	−4.0	−0.6	−29.9
Average			1.12	0.05	5.36	21.2	0.07	1.21	100	425	−8.0	−1.6	−30.6
Median			1.07	0.05	5.79	22.0	0.06	0.75	88	425	−8.1	−1.4	−30.7
FP9	Bs2	–	–	–	–	–	–	–	–	–	–	–	−32.0
FP10		–	–	–	–	–	–	–	–	–	–	–	−31.8
Z/10"'		–	–	–	–	–	–	–	–	–	–	–	–
Z/10"		18.4	2.79	0.11	4.58	24.7	0.18	8.90	319	420	−2.8	−4.1	–
Z/10'		–	–	–	–	–	–	–	–	–	–	–	–
Z/15		17.7	3.53	0.13	5.49	26.2	0.27	17.30	490	419	−4.8	−3.9	–
FP24B		12.3	3.11	0.12	5.85	26.7	0.15	13.30	428	422	−3.5	−3.4	−32.6
FP24A		12.2	2.41	0.10	4.69	24.5	0.13	9.42	391	419	−3.5	−3.4	−32.6
FP11		–	–	–	–	–	–	–	–	–	–	–	−32.9
5/19		11.5	1.84	0.08	2.28	23.2	–	–	193	411	−5.1	−2.2	–
FP7		–	–	–	–	–	–	–	–	–	–	–	−32.4
FP6		–	–	–	–	–	–	–	–	–	–	–	−31.9
FP5		–	–	–	–	–	–	–	–	–	–	–	−31.8
5/18		11.2	1.90	0.09	2.16	21.1	0.10	2.33	123	410	−6.6	−3.4	
FP4		–	–	–	–	–	–	–	–	–	–	–	−32.7
FP3		–	–	–	–	–	–	–	–	–	–	–	−32.7
5/17		10.9	1.79	0.08	2.26	21.9	0.12	2.84	158	415	−4.9	−2.0	–
FP23B2		10.8	1.44	0.07	2.95	21.2	0.08	2.70	188	421	−3.3	−2.6	−32.8
FP23B1		10.7	1.46	0.07	2.92	21.9	0.08	3.30	226	419	−3.5	−2.6	−32.8
FP23A		10.7	0.56	0.04	5.87	13.8	0.04	0.49	87	415	−18.1	−1.7	−32.0
Min			0.56	0.04	2.16	13.8	0.04	0.49	87	410	−18.1	−4.1	−32.9
Max			3.53	0.13	5.87	26.7	0.27	17.30	490	422	−2.8	−1.7	−31.8
Average			2.08	0.09	3.90	22.5	0.13	6.73	260	417	−5.6	−2.9	−32.5
Median			1.87	0.09	3.76	22.6	0.12	3.30	209	419	−4.1	−3.0	−32.6
FP19	Bs1	0.6	0.91	0.03	6.40	31.5	0.04	0.37	41	443	−9.0	0.7	−30.5
FP18B		0.5	0.76	0.04	4.91	18.3	0.03	0.49	64	423	−7.5	0.7	−32.9
FP18A		0.5	0.96	0.05	4.26	19.4	0.05	0.66	68	425	−9.8	0.1	−33.4
FP17		0.3	1.06	0.06	1.69	18.1	0.05	0.93	88	423	−5.8	−1.8	−33.6
FP16B		0.3	0.86	0.04	4.70	20.8	0.05	0.74	86	422	−6.1	0.5	−33.1
FP16A		0.2	0.74	0.04	4.04	16.6	0.03	0.78	106	421	−5.9	0.9	−32.5
FP16		0.2	0.59	0.04	4.50	15.1	0.04	0.41	70	423	−6.1	1.1	−32.8
FP15		0.1	0.85	0.06	1.96	14.0	0.04	0.65	76	421	−5.1	−1.3	−32.6
FP8		0.05	–	–	–	–	–	–	–	–	–	–	−33.3
Min			0.59	0.03	1.69	14.01	0.03	0.37	41	421	−9.8	−1.8	−33.6
Max			1.06	0.06	6.40	31.50	0.05	0.93	106	443	−5.1	1.1	−30.5
Average			0.84	0.05	4.06	19.23	0.04	0.63	75	425	−6.9	0.1	−32.7
Median			0.85	0.04	4.38	18.22	0.04	0.65	73	423	−6.1	0.6	−32.9

Chitinite occurs in Bs2, but the other zooclasts like fish bone particles are present in the main ore bed.

5. Discussion

Huge black shale-hosted Mn-carbonate deposits offer a special opportunity for determining paleo-oxygen levels. Low-temperature aqueous Mn(II) oxidation takes place via bacterial activity by a two-step enzymatic process that requires oxidative conditions (Tebo et al., 2004; Webb et al., 2005; Bargar et al., 2005), which for the Úrkút took place during accumulation of the Mn(IV, III) oxide proto-ore. Black shale formation in the Úrkút basin was likely the result of moderate productivity (Table 3A) caused by bacterially mediated reactions and plankton productivity, which upon burial underwent decomposition of the reactive marine organic matter via Mn(III, IV) reduction. The high productivity proposed by Vető (1993), Vető et al. (1995), and others may have inhibited the colonization of the basin by benthic fauna, even under moderate upwelling conditions. However, as indicated by our data, lamination and the lack of benthic fauna occurred even with oxic bottom waters and moderate primary productivity. Vető (1993) also concluded that the Úrkút basin in the early Toarcian sea did not contain H_2S and had oxic bottom waters, which is also supported by the size distribution of framboidal pyrite (Polgári et al., 2016).

5.1. Chemical composition and multi-proxy paleoenvironmental geochemistry

Chemical, enviromental. and genetic proxies indicate formation of the black shale under oxic to sub-oxic bottom-water conditions, high to moderate surface-water productivity, typical marine conditions, low terrigenous input, and no direct magmatic hydrothermal input. The proxies for the black shale sections Bs1, 2, 3-4 and the Mn-carbonate ore beds show strong similarities (Table 3A). The Úrkút black shale formed predominantly under suboxic bottom-water conditions and experienced anoxia only during early diagenesis, by microbially mediated sulfate reduction and pyrite formation (Polgári et al., 2016).

Neuendorf et al. (2005) described black shale as a laminated, organic-rich shale with 5% or more carbon content that also contains sulfides (usually pyrite) and elevated concentrations of some such as

U, V, Cu, and Ni. Though the Úrkút black shale is laminated and contains pyrite, its organic carbon content is lower than 5% and it is depleted in V, U, and Ni relative to standard shale. The EF of Cu is only 3. Co shows some enrichment in pyrite and Sr is enriched in barite; Ba averages 307 ppm, with a maximum of 3020 ppm (Polgári et al., 2003a). Co, Ni, As, and REE enrichments are related to disseminated grains a few tens of micrometers in size, e.g., Co-, Ni-, Ag-sulfide, and Co- and Ni-bearing pyrite, which are mainly in the black shale underlying the main carbonate ore bed (Bs1). Based on bioproductivity proxies (P, Ba) and redox elements like Cr, Co, Ni, Cu and Pb, the MRV-ÓSF sites were enriched, which is similar for the Úrkút shale for Cu and Co, but not for Cr, Ni and Pb (Raucsik and Merényi, 2000).

Kearey (2001) gave a similar definition for black shales based on organic matter content and indicated that they generally formed under anoxic marine bottom-water conditions. This definition does not fit the Úrkút depositional environment, where the black shale sediment was deposited under oxic bottom waters (Polgári et al., 2013a, 2016). The organic matter content of T-OAE black shales is highly variable, but often below 2 wt.% (Jenkyns, 1988). Jenkyns (1988) emphasized that the Mn-rich black shales contain much less organic matter (around 5 wt.%), than the metal-free black shales. It is essential to distinguish ore-bearing and non-ore-bearing black shales and to further distinguish sulfidic ore-bearing and Mn-carbonate ore-bearing black shales, because their redox and other environmental conditions were different. The Úrkút black shale generally follows the observations of Jenkyns (1988), but has even less organic matter (Table 4) than he indicated, and does not fit with the idea of anoxic marine bottom waters (Table 3A).

Most of the Toarcian black shales have been studied for organic compounds but inorganic geochemical data are scarce, which does not allow for detailed comparisons. Enrichment factors >5 for the Posidonia Shale occur only for S and Sc with a maximum for S of 11.5, whereas for the Úrkút black shale, the enriched group of elements is much greater (Te, Co, S, As, Mn, Mo, Ca) (Table 3B), with a maxima for Co (15.0) and Te (17.4) (João et al., 2012). The elements depleted relative to average shale are In, Hf, K, Ba, and Na for the Úrkút black shales, which compares with the Posidonia Shale for K, Na and Ba, but not for Sb, Rb, Ti, Zr, Mg, Mn, which are depleted in the Posidonia Shale.

Paleoproxy redox indicators (Ni/Co, V/Cr, V/V + Ni), $Mn^* = \log [(Mn/Mn_{PAAS})/(Fe/Fe_{PAAS})]$; Taylor and McLenmann, 1995) indicate oxic conditions for the Úrkút depositional basin. However, results of paleoredox indicator element ratios must be used with caution because of microbial selective element enrichments and mobilizations, so it is recommended to include interpretations based on mineralogy and microtextures to determine consistency with these proxies (Bíró et al., 2015).

Microtextures show that partly pyritized Fe-rich biomats in the Úrkút black shale characterize the entire sections. This observation also applies to the Mn ore. Fe-rich biomats form under suboxic (Eh: +0.3 V) neutrophylic conditions (Fig. 5), which fits well with conclusions from Fortin et al. (1997), Konhauser (1998), and Konhauser (2012). The Úrkút black shale is fine grained, and silty terrestrial debris does not occur, consistent with our interpretation of the microtextures.

5.2. Mineralogy of the black shales

Previous studies of the Úrkút Mn-carbonate ore deposit, preliminary investigations of the black shale host rock, together with data presented here provide a comprehensive understanding of the mineralogy. Further, this offers an opportunity for comparisons with other black shales, among them epicontinental shelf black shales of Toarcian age.

The black shale mineral assemblage is similar to that of the ore beds, reflecting similar formation conditions, but the minerals occur in different amounts that determine whether the rock is ore or waste. The minerals consist of (i) Carbonates, like *calcite* (*Mn-calcite*) occurring in the form of biogenic debris of variable size, mainly of plankton and nekton, rarely benthic forms (Polgári et al., 2012a). *Dolomite* grains with a size of tens of micrometers (often idiomorphic) and showing Mn-metasomatism at the margins of the grains. There are two ideas as the origin of these dolomite grains: (1) windblown particles from sabkha facies (Pekker, 2005); and (2) early diagenetic products of microbially mediated carbonate formation and diagenesis (Dupraz and Viesscher, 2005, Pace et al., 2015; Molnár, 2015 adapted Dupraz and Visscher's model for the Úrkút). *Rhodochrosite* is a very fine-grained microbially mediated early diagenetic mineral, as well as *siderite* (Polgári et al., 1991). Negative $\delta^{13}C$ values of carbonate support an organic matter contribution to the mineralization under suboxic

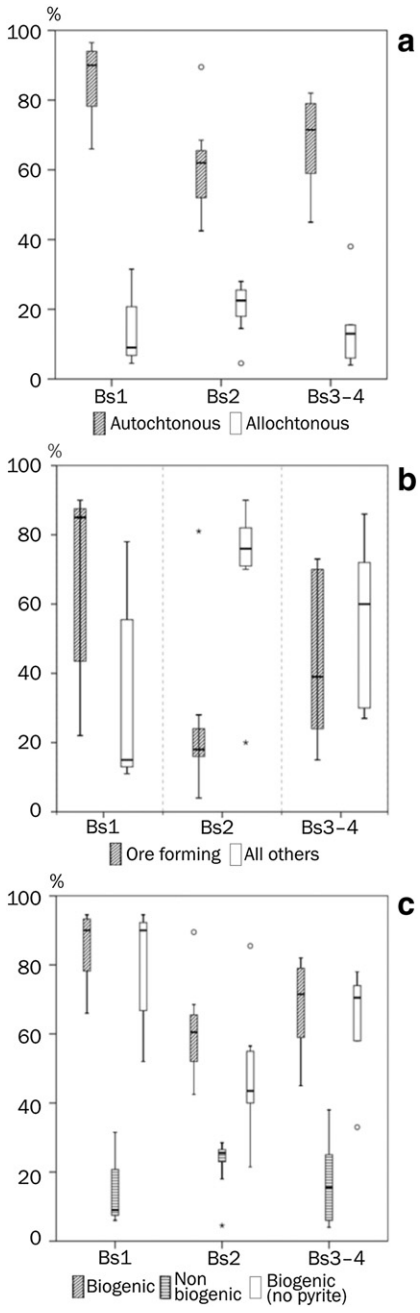

Fig. 7. Box plot diagrams of authigenic and detrital phases (a), components from ore-forming processes (b), and biogenic components (c). Legend: the boxes show the distance between the lower and upper quartiles (above and below them 0.25% and 0.75% of the values can be found), and the black line in the box is the median. The vertical lines show the 1.5 distance from quartiles values. Those values which are above or below this line are the outliers (o), and those, which are above or below the outliers are the extreme values (*).

conditions in the zone of manganese reduction (Table 3). *Kutnohorite* occurs as vein fillings and impregnations that formed during a later diagenetic stage (Polgári et al., 2007). (ii) Oxides like *quartz* have several origins based on textural characteristics, windblown particles, authigenic precipitation, and recrystallized biodebris such as radiolarian tests. Diagenetic segregation of quartz is also noted (Polgári et al., 2012a, 2016; Molnár, 2015). *Goethite* occurs as biomats (Polgári et al., 2012b). (iii) Phyllosilicates like *smectite* and *celadonite,* are authigenic (Weiszburg et al., 2004a,b; Tóth et al., 2010; Polgári et al., 2013a). The clay minerals were proposed to have formed by direct precipitation onto microbial cell organic matter and EPS, which resulted in clay-rich primary phases, later accompanied by carbonate precipitation via early diagenesis (Yeshaya and Moshe, 1988; Zavarzin, 2003; stated also for Úrkút by Molnár, 2015). Though the Úrkút black shale-hosted Mn mineralization was mediated by various types of microbial activity (Polgári et al., 2010, 2012a,b), it is feasible that the Mn mineralization could have also resulted from high amounts of primary authigenic clay mineralization. In this interpretation, the microbially induced and controlled processes cannot be distinguished. We consider celadonite and smectite as authigenic (Cora, 2009; Tóth et al., 2010; Polgári et al., 2013a), possibly microbially mediated products, while chlorite, kaolinite, and unspecified clay minerals are considered detrital. *Chlorite* and *kaolinite* represent rare terrigenous input (windblown). Tectosilicates like *K-feldspar* and *plagioclase* originated from volcanic ash falls based on cathodoluminescence evidence (Polgári et al., 2012a). *Zeolite* (*clinoptilolite*) can result from ash alteration (Polgári, 2001), but has been also shown to fill algal cells (Cora, 2009). (iv) Sulfides, like *pyrite* are a common constituent of early diagenetic processes in the zone of sulfate reduction; (v) Sulfates, like *barite* formed as an early diagenetic mineral via plankton decomposition (Polgári et al., 2016). (v) *Gypsum* is the product of alteration of pyrite (Polgári et al., 2012a). (vi) Phosphates *like Apatite* occur as fish debris, and in some black shale layers its concentration is very high (Polgári et al., 2003b, 2007, 2012a).

The scarce data available on the mineralogy of black shale-hosted Mn indications of the Alpine–Mediterranean region are similar to that characteristic for the Úrkút, like diagenetic rhodochrosite and authigenic smectite and celadonite (Cornelius and Plöchinger, 1952; Gruss, 1956; Polák, 1957; Andrusov, 1965; Germann and Waldvogel, 1971; Germann, 1971; Bernoulli and Jenkyns, 1974; Faupl et al., 1982; Beran et al., 1983; Jenkyns, 1988; Jenkyns et al., 1991; Krainer et al., 1994; Krajewsky et al., 2001; Rantitsch et al., 2003; Jach and Dudek, 2005). In contrast, the mineralogical composition of black shales formed on epicontinental shelves differs from the Úrkút, containing mainly detrital components.

The Toarcian Jet Rock Formation (UK), contains considerable amounts of detrital minerals (Morris, 1980) like muscovite (5–7%), biotite, and chlorite, which are not characteristic for Úrkút, but high amounts of quartz and rare feldspar contents are similar. The high clay mineral content is also similar to Úrkút, but the types of clay minerals are different. For example in the Jet Rock, the illite and mixed-layer clay minerals represent 55–60%, kaolinite is also high, 35–40%, chlorite is 5%, vermiculite is a trace, and smectite, which is considerable in Úrkút, does not occur in the Jet Rock Formation.

Similarly, the Posidonia Shale of the Dutch Central Graben contains silt-size detrital quartz, dolomite, and kaolinite, rare alkali feldspar, and abundant pyrite, quartz silt, and clay minerals, which constitute

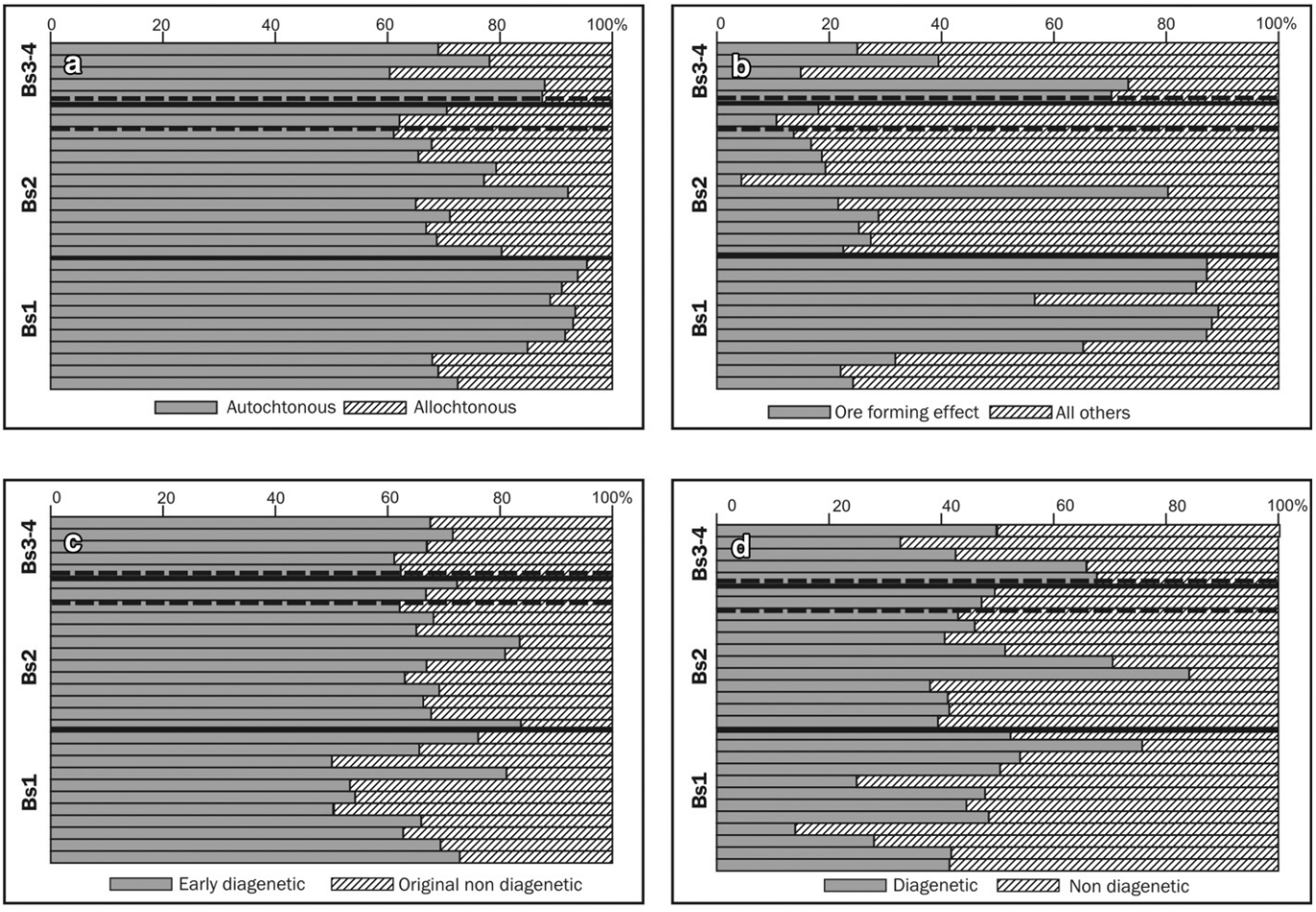

Fig. 8. Contributions from various sources and processes on black shale mineralogy. For details see Table 5. Bold black lines represent ore horizons, bold dashed lines represent hiatus in black shale sections.

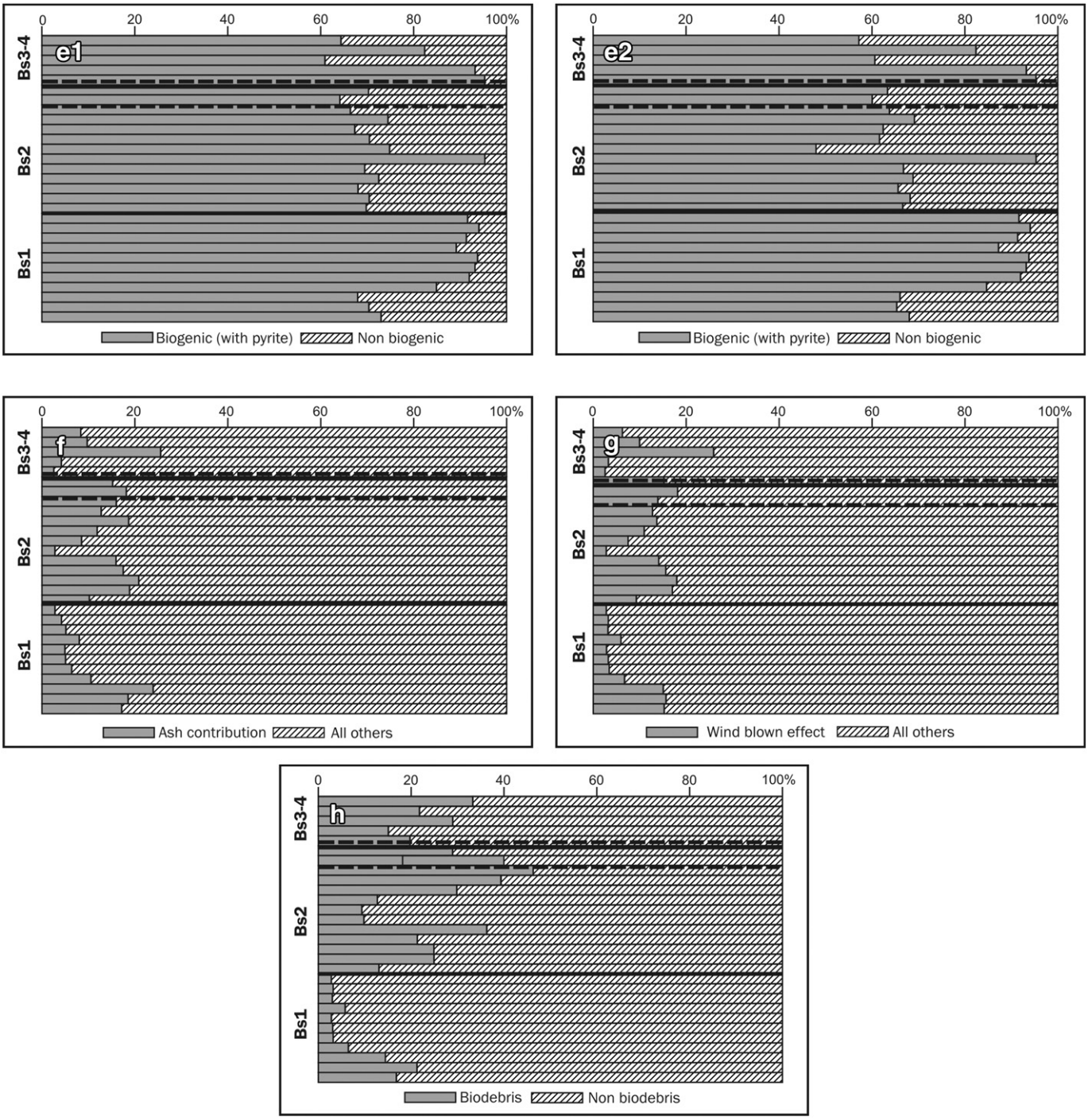

Fig. 8 (*continued*).

most of this and other epicontinental shales (João et al., 2012). The shales contain little carbonate except for authigenic dolomite while in Úrkút contains high amounts of rhodochrosite, which is also characteristic of the black shale. Minor diagenetic dolomite occurs in the Úrkút black shale.

The samples collected from the black shale section of the MRV-ÓSF are predominantly composed of calcite, quartz, kaolinite, illite ± muscovite, and bituminite material (Raucsik and Varga, 2008b). Additionally, pyrite, illite/smectite mixed-layer minerals, chlorite, rare plagioclase and K-feldspar are also present. Moreover, there are some secondary minerals such as goethite and gypsum, reflecting outcrop weathering. The clay fraction of the MRV-ÓSF black shale samples is dominated by kaolinite (Raucsik and Varga, 2008a) 50–80%, average 67.5% and illite (15–50%, average 30%); random I/S mixed-layer minerals occur in small quantities (from trace amounts to 5–10%), in places with traces of chlorite. Hence, in contrast to the Úrkút, the MRV-ÓSF black shale contains mainly detrital components. Based on clay mineralogy, Raucsik and Merényi (2000) inferred the connection between an upwelling system and climate change (more humid) of the provenance area for the MRV-ÓSF black shale, which does not apply to the Úrkút because of the predominance of authigenic minerals.

Dera et al. (2009) assessed the Europe-wide distribution of clay minerals deposited through the late Pliensbachian and early Toarcian and recognized that significant kaolinite enrichment occurred within the *falciferum* Zone, broadly coeval with the $\delta^{13}C$ excursion on epicontinental shelf areas. This relative increase in kaolinite abundance was

interpreted as evidence for highly efficient continental runoff under a warm, humid climate, which did not reach the Úrkút basin.

5.3. Calculation of environmental conditions based on mineral composition

Both the black shale and the ore are composed mainly of authigenic minerals together with calcite biodebris, ash, and other windblown particles (Table 2). Some authigenic and terrigenous detrital minerals were preserved while others were transformed to other minerals during diagenesis. Formation of various authigenic and diagenetic minerals occurred through both microbially mediated processes and through inorganic processes. A starved basin with variable but dominant authigenic mineralization was determined by quantification of mineral assemblages. The authigenic mineral content exceeds the terrigenous (allothigenic) content in all the black shale beds; in Bs1 this ratio is ~90:10, and is also high in Bs2 (~60–40), and Bs3-4 (~70–30) (Table 2; Figs. 7a, 8a). Based on different distributions of the minerals, the environmental conditions during black shale formation can be inferred (Table 5). The ore-forming stages are summarized on Figs. 7b, 8b, which indicate that the processes of ore formation started at a very early stage and represent important contributions in all the black shale beds. The ore-forming processes were the strongest in Bs1, where as much as 85% of the black shale is composed of authigenic minerals related to ore formation, though the data show high variability, down to 15%. The ore-forming processes decreased in Bs2 (17%) and increased again in Bs3-4 (35–40%). This does not mean that all the authigenic minerals formed are ore minerals. Along with the authigenic ore-forming minerals, background sedimentation of the black shale continued (Fig. 8c) and the whole system was affected by diagenesis (Fig. 8d). Microbially mediated chemical reactions were involved in the formation of all the black shale beds, such as contributions of authigenic biogenic minerals from 60 to 90% including pyrite, or 45–90% without pyrite (Figs. 7c, 8e1-2). Ash sedimentation also comprises up to 30% of some beds (Fig. 8fg). Biodetritus represented by calcite tests was a basic constituent comprising up to more than 40% of some beds (Fig. 8h).

The black shale basin was a structurally controlled starved depocenter because deep ocean between the continent and the Úrkút basin blocked most terrestrial input. The main mass of sediment that comprises the black shale is authigenic clay and ore minerals that originated most probably from geothermally generated hydrothermal fluids, which has also been proposed as the source of the metals (Polgári et al., 2012a). These processes took place from the beginning of the change from limestone/marlstone deposition to deposition of Bs1, but the ore did not form immediately, probably because the oxygen supply for enzymatic Mn(II) oxidation was insufficient. However, Mn carbonate-rich laminae did form in the Bs1 very close to its contact with the underlying carbonate. The sharp contact between the limestone/marlstone footwall and the ore deposit, initiated during formation of Bs1, could have resulted from the enzymatic oxidation of a huge amount of Mn and Fe. This was a process that reduced the pH that blocked carbonate formation, which is consistent with the research of Ehrlich (2015). At the same time, the venting fluids produced authigenic clay minerals directly on organic matter and EPS as described by Yeshaya and Moshe (1988) and Zavarzin (2003). The accumulation of microbially produced highly reactive organic matter resulted in a mass-balance change after burial and, during early diagenesis; the sediment became anoxic in the zone of sulfate reduction where pyrite formed. A major part of the organic matter is found in a highly decomposed form of bituminite and lamalginite in the section, while the ratio of the more resistant macerals to microbial attack like vitrinite, inertinite and telalginites relatively increased. Other minerals like barite and zeolite also formed during early diagenesis. Paleoproxy calculations indicate that similar conditions existed during accumulation of the black shale and the ore (Table 3).

A distal hydrothermally and microbially induced clay mineral-rich authigenic assemblage (marlstone) is an accurate description of the black shale, in which distinct Mn-carbonate ore beds (Mn-rich laminae) formed from close to the very beginning, when the oxygen supply in the sedimentary basin was high enough for enzymatic Mn(II) oxidation (enzymatic Mn(II) oxidation engine; Fig. 9). Hydrothermal activity cannot be excluded as a mechanism for initiation of ore deposition.

Our results concerning oxygen supply are different than that of the Jet Rock Formation, which accumulated in poorly oxygenated bottom waters, and consequently has high organic carbon contents, 11.8% (max: 35%; Morris, 1980), much higher than the Úrkút. The Posidonia

Table 5
Effects and calculation on accumulation based on mineralogy.

Legend	Process	Minerals used for calculation	Minerals used for calculation
a	**Starved basin, lack of terrestrial detrial input**	**Authigenesis**	**Allochtonous**
		q/2*, sid, bar, zeol, smec, cel, dol, rhod, pyr, cal/2**	chl, kaol, clay, plag, K-fp, q/2, cal/2
b	**Ore forming processes**	**Ore forming minerals**	**Non-ore forming**
		sid, smec, cel, rhod	bar, zeol, pyr, kut, chl, kaol, clay, plag, K-fp, dol, cal, q
c	**Background black shale sedimentation**	**Early diagenetic**	**Original non-diagenetic**
	Ore forming minerals not considered here	2q/3, cal/2, pyr, zeol, bar, dol, kut	q/3, chl, kaol, clay, plag, K-fp, cal/2
d	**Effect of diagenesis**	**Diagenetic**	**Non-diagenetic**
		q/2, rhod, kut, pyr, zeol, bar, sid, dol, cal/2	q/2, chl, kaol, clay, cel, smec, plag, K-fp, cal/2
e/1	**Effect of microbial mediation (with pyrite)**	**Biogenic (with pyrite)**	**Non-biogenic**
		rhod, sid, pyr, q/2, dol, smec, cel	bar, zeol, kut, chl, kaol, clay, plag, K-fp, q/2
e/2	**Effect of microbial mediation (no pyrite)**	**Biogenic (no pyrite)**	**Non-biogenic**
	cal/2 as biodebris not considered here	rhod, sid, q/2, dol, smec, cel, cal/2	bar, zeol, kut, chl, kaol, clay, plag, K-fp, q/2
f	**Ash contribution**	**Ash contribution**	**All others**
		q/3, plag, K-fp	2q/3, smec, cel, chl, kaol, clay, sid, cal, rhod, kut, pyr, zeol, bar, dol
g	**Windblown contribution**	**Windblown**	**All others**
		q/3	2q/3, plag, K-fp, smec, cel, chl, kaol, clay, sid, cal, rhod, kut, pyr, zeol, bar, dol
h	**Biodebris contribution**	**Biodebris**	**Non-biodebris**
		q/3, cal	2q/3, plag, K-fp, smec, cel, chl, kaol, clay, sid, rhod, kut, pyr, zeol, bar, dol

See text for origin of the different minerals, and Fig. 8.
q—quartz; plag—plagioclase, K-fp—K-feldspar; smec—smectite; cel—celadonite; chl—chlorite; kaol—kaolinite; clay—not determined in detail; sid—siderite; cal—calcite; rhod—rhodochrosite; kut—kutnohorite; pyr—pyrite; zeol—zeolite; bar—barite; dol—dolomite; clay—unspecified clay minerals
q/2*: concerning the multiple origin of quartz, the /2, /3 shows the rate which was taken into consideration in the given calculation; e.g. q/2 means 50% of quartz; 2q/3 means 2/3 part of quartz, etc.
cal/2**: concerning the multiple origin of calcite, similar calculation was made as in the case of quartz.

Samples	Mineralogy		Oxygen supply			
	marker minerals of diagenetic anoxic conditions	marker minerals of oxic conditions	anoxic (DO: 0 mL/L	suboxic (DO: 0 – 0.2 mL/L	dysoxic (DO: 0.2 – 2.0 mL/L	oxic (DO: > 2 mL/L
		microbially mediated diagenetic rhodochrosite and siderite	Eh: -0.2 - 0 V	Eh: 0 – 0.2 V	Eh: 0.2 - 1 V	>1 V
			diagenetic		syngenetic	
					Fe-rich biomat formation (Eh: 0.3 V)	Mn oxide proto minerals
chert/ironstone hanging wall						
FP21	pyrite	rhodochrosite	diagenetic pyrite formation via microbially mediated sulphate reduction	diagenetic microbially mediated rhodochrosite and siderite formation		
FP22	pyrite	rhodochrosite, siderite				
- - - - - - - - - - -		- - - - - - - - - - -			- - - - - - - - - - - -	- - - - - - - - - - - -
Mn carbonate ore bed						
FP9	pyrite					
FP10	pyrite					
- - - - - - - - - - -		- - - - - - - - - - -			- - - - - - - - - - - -	- - - - - - - - - - - -
FP24B	pyrite	rhodochrosite				
FP24A	pyrite	rhodochrosite				
FP11	pyrite					
FP7	pyrite					
FP6	pyrite	rhodochrosite				
FP5	pyrite	rhodochrosite				
FP4	pyrite					
FP3	pyrite	rhodochrosite				
FP23	pyrite	rhodochrosite				
Mn carbonate ore bed						
FP19		rhodochrosite				
FP18	pyrite	rhodochrosite				
FP17	pyrite					
FP16						
FP15	pyrite					

Fig. 9. Syngenetic oxygen supply based on mineralogy.

Shale shows that organic matter accumulation and preservation, high bioproductivity, continuous or periodic anoxia, and high sedimentation rates were closely connected with paleoenvironmental changes in the shallow-water sedimentary basin (Röhl et al., 2001; Schmid-Röhl et al., 2002; João et al., 2012). Kemp and Kentaro Izumi (2014) reported similar conditions (shallow-water, fluvial course-grained terrestrial

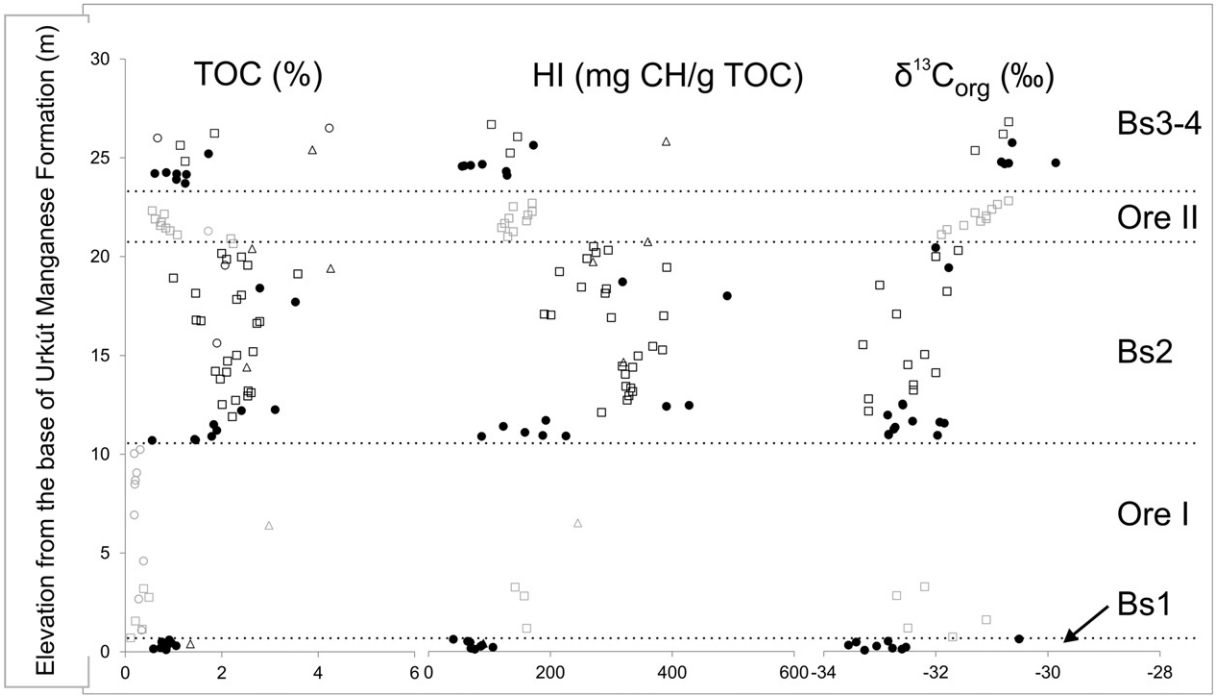

Fig. 10. Total organic carbon (TOC), Hydrogen Index (HI) and kerogen carbon isotope values. (Bs = black shale). Dots: current samples; circles: data from Polgári et al. (1991); squares: data from Vető et al. (1997), triangles: data from Polgári et al. (2000). Vertical axis: distance from the footwall Isztimér Limestone.

debris contributions) for a section deposited on the northwestern margin of Panthalassa and now exposed in southwest Japan. These examples contrast with the Úrkút basin, which was deeper water, under storm wave base.

According to Raucsik and Varga (2008b) and based on Jenkyns (1985), the MRV-ÓSF black shale formed under intense upwelling and high plankton productivity, which caused the accumulation of large amounts of organic matter in the epicontinental sea on the European shelf. Though upwelling and moderate to high productivity was determined for the Úrkút basin, and also a similarity in marine algae origin of the organic matter exists, the Úrkút shale accumulated under a different tectonic regime, a pelagic marine environment along a rifting continental margin, which fits well with comparable scenarios described by Bernoulli and Jenkyns (1974), Jenkyns et al. (1991), Channell et al. (1992), and others.

5.4. Organic geochemistry

Vető et al. (1995) determined a predominantly marine algal origin for the organic matter, which fits well with our data for the Bs2 section. However, different features of Bs2 compared to Bs1 and Bs3-4 indicate a change in OM deposition although differences are too small to be interpreted on the basis of our preliminary data. Present results show a quasi-uniform, mixed terrestrial and marine origin of immature OM in all the black shale beds, with additional contributions of algae or bacteria to the Bs2 OM complement. Possible trends in Bs2 suggest that study of the central parts of Bs2 would be fruitful, but sampling would require a tunnel driven in the mine.

Major components of maceral composition along the whole Úrkút section (including the ores) are liptinites (bituminite and liptodetrinite), with a 10–12% contribution of laminated alginite. Vitrinite and inertinite also occur, but only as minor components. Intense biodegradation of trace fossils and relative increase of liptinites (Tasmanites-type solitary alga) can be observed in the ore, due to the in situ oxidation and consumption of less resistant bituminite, laminated alginate, and liptodetrinite of planktonic origin (Hámor-Vidó, 2015). A less intense decomposition of bituminite and laminated alginite (together with the transformation of pyrite to iron oxyhydroxides), as described in the MRV-ÓSF, is interpreted as a late-stage oxidation of the section by Varga et al. (2007). They stated that the maceral

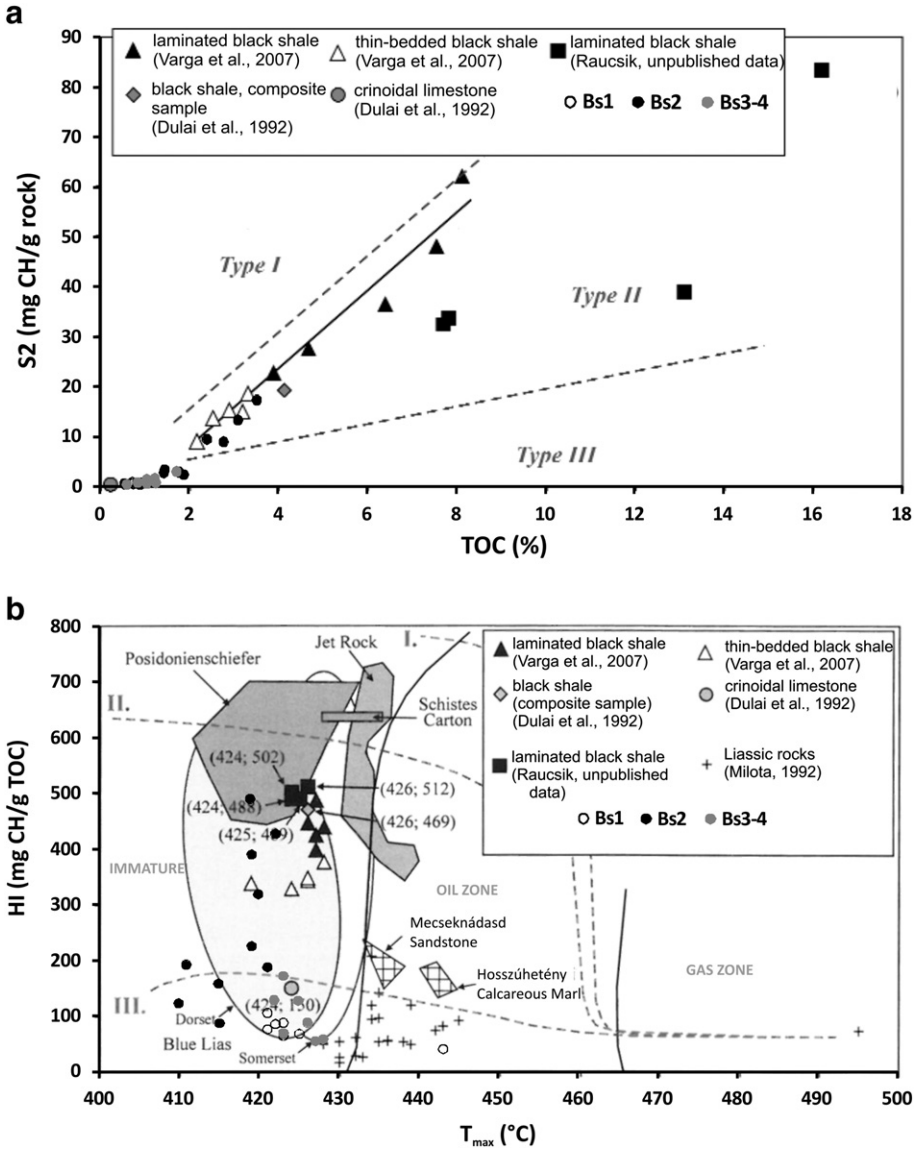

Fig. 11. Comparison of kerogen type (a, b) and maturity (b) of Bs1, Bs2 and Bs3-4 with data from Varga et al. (2007) and other black shale deposits cited therein. The loss of hydrogen-rich algal biomass during diagenesis results in type III kerogen values. Data from Hollander et al. (1991), Dulai et al. (1992), Milota (1992), Katz (1994), Sælen et al. (2000), Röhl et al. (2001), Schmid-Röhl et al. (2002), Deconinck et al. (2003), Varga et al. (2007).

composition of the black shale and the underlying calcareous marl are similar to the Úrkút black shales: liptinite (bituminite, alginate, liptodetrinite) is dominant (above 95%), and the organic-matter content is higher in the black shales than in the marlstone. For both in Úrkút and MRV-ÓSF, the bituminite content is the highest in the black shales with flaser texture (Varga et al., 2007; Hámor-Vidó, 2015).

The medium to low HI values of the immature OM (Polgári et al., 1992) reflect oxidative loss of hydrogen-rich marine OM during diagenesis, thus precursor OM is assumed to be type II kerogen through the whole section (Fig. 10). Maceral composition and traces of non-aromatic hydrocarbons show limited terrestrial contributions, which corroborates this assumption.

Comparing our data with those of Hollander et al. (1991), Katz (1994), Sælen et al. (2000), Röhl et al. (2001), Schmid-Röhl et al. (2002), Deconinck et al. (2003), and Varga et al. (2007), we can see significant differences between the sample sets studied (Fig. 11). Bs1 and Bs3-4 are characterized by low TOC, S2, and HI compared to black shales of the MRV-ÓSF (Varga et al., 2007). T_{max} values are in the same range (<430 °C) reflecting immaturity of OM in both sample sets. Unlike the MRV-ÓSF black shale, only some of Bs2 samples reach the range of fair or better source-rock potential. We have to note that the MRV-ÓSF black shales are considered to be weathered, which caused the measured S2 and HI to be lower than the original (Hollander et al., 1991; Katz, 1994; Sælen et al., 2000; Röhl et al., 2001; Schmid-Röhl et al., 2002; Deconinck et al., 2003; Varga et al., 2007).

Fig. 12a, b shows comparisons of our samples with significant Toarcian black shales (Posidonia Shale, Jet Rock, and Schistes Carton of the Paris Basin) based on carbon isotopic compositions of organic matter, TOC, and HI. No obvious differences occur but HI and TOC values are smaller in the black shale samples, except for two Bs2 samples, and the $\delta^{13}C_{Corg}$ (VPDB) values of Bs1 and Bs2 differ from those of otherwise comparable Toarcian shales, except for some Posidonian Shale samples. Bs3-4 samples differ partially as well but with more overlap (Hollander et al., 1991; Katz, 1994; Sælen et al., 2000; Schmid-Röhl et al., 2002; Röhl et al., 2001; Deconinck et al., 2003; Varga et al., 2007).

The isotopic composition of carbonate in the Úrkút black shale also differs from that of MRV-ÓSF black shale (Fig. 13). Here, we observed that oxygen isotopic compositions vary by about −2‰ (−5‰ to −2‰ SMOW), and $\delta^{13}C$ values range from −2‰ to −12‰ (VPDB), with one exceptionally negative Bs2 sample. Varga et al. (2007) concluded that the isotopic compositions of carbonate from MRV-ÓSF black shale, $\delta^{13}C$ −6‰ to 0‰ (VPDB) and $\delta^{18}O$ −4‰ to −13‰ (SMOW), reflect a high water-to-rock ratio and homogenous late-stage diagenetic fluids. Thus, these isotopic values cannot be used to assess temperature and salinity of the depositional basin or early diagenetic environment.

High values of TOC and HI are found more than a meter above the main ore bed-Bs2 boundary up to the base of second ore bed, such as the inner parts of Bs2 contain better preserved OM. A weak correlation exists between carbonate content and carbon isotopic composition. The increase of carbonate generation is connected to the bacterial decomposition of reactive algal OM, and isotopically light carbon is incorporated into the carbonate formed. We can assume that the variation of the data is probably due to the periods of ore formation, which are governed by

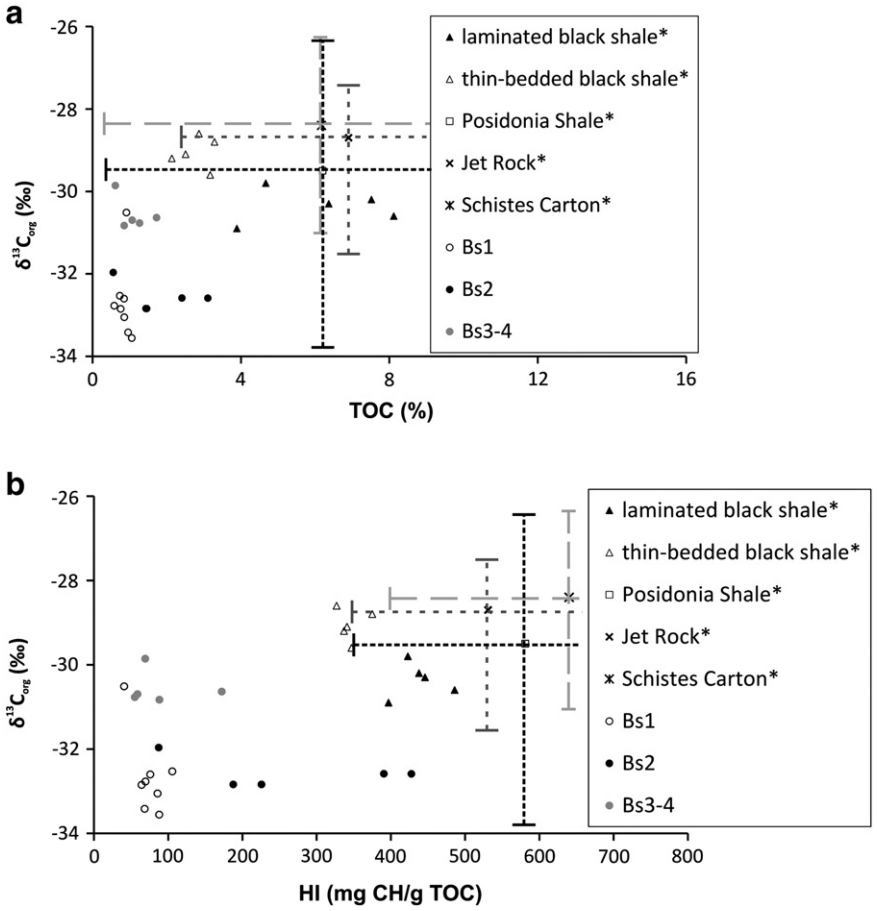

Fig. 12. Carbon isotopic compositions versus TOC (a) and HI (b) values with data from Varga et al. (2007). Dashed lines represent the ranges of data. Significant differences between Úrkút (Bs1, Bs2 and Bs3-4) and other deposits can be seen. *Data from Hollander et al. (1991), Katz (1994), Sælen et al. (2000), Schmid-Röhl et al. (2002), Röhl et al. (2001), Deconinck et al. (2003), Varga et al. (2007).

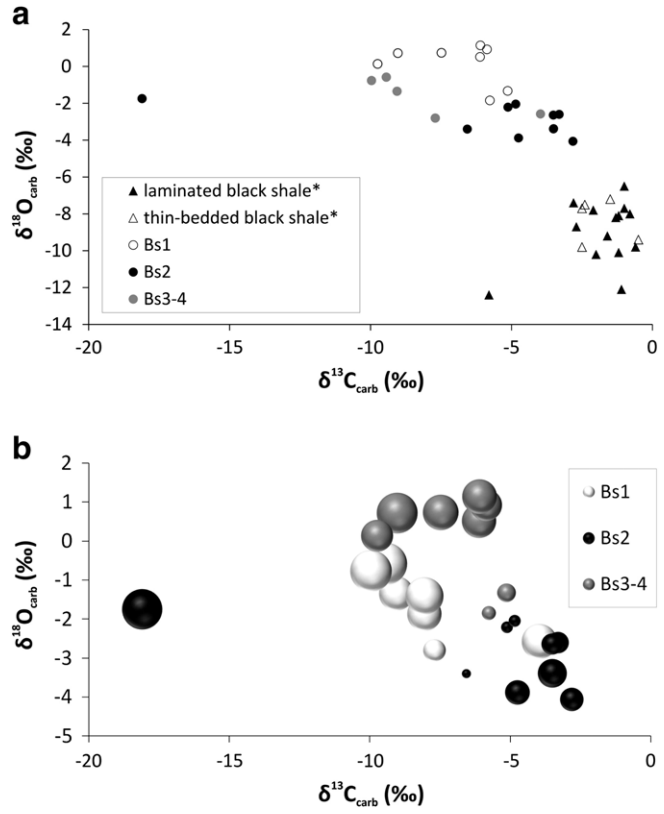

Fig. 13. Carbon and oxygen isotopic composition of carbonates; (a) comparison with MRV-ÓSF black shale (*data from Varga et al. (2007)), (b) diameter of the dots represents carbonate content (~2–50 wt.%), showing the more negative values of carbonate-rich samples, Úrkút black shale.

changes in the redox conditions at the sediment-water interface. The pristane to phytane ratio (Pr/Ph) in the black shales falls between 0.77 and 1.01 suggesting also an anoxic-dysoxic diagenetic environment (Polgári et al., 2000). However, non-bacterial carbonate formation cannot be excluded, especially in the Bs3-4 section.

We cannot exclude that the OM of the MRV-ÓSF black shale and Úrkút black shales originated from similar precursor organic matter, with differences in paleogeography (e.g. decrease of salinity in the MRV-ÓSF black shale), and a major difference being ore mineralization, which did not take place in the MRV-ÓSF black shale. However, the differences in the geochemistry of OM do not reflect distinct depositional environments and perhaps resulted from the partial oxidation and biodegradation (bacterial consumption of) H-rich OM to form Mn and Fe-carbonates, and some pyrite, and they reflect the low preservation of primary liptinites and the elevation of decomposed constituents of fluorescing and non-fluorescing bituminites.

We note that the presence of a carbon isotopic excursion (CIE) representative of the Toarcian Oceanic Anoxic Event (T-OAE) cannot be verified in the Úrkút section even though Úrkút deposition occurred during that time interval. Two plausible explanations are offered: Polgári et al. (2012b) suggested an extremely fast (several hundred years) process of ore formation and sedimentation in the main ore bed, so that the whole process may have taken place over a small time interval during the T-OAE. This would explain the relatively negative $\delta^{13}C_{PDBCorg}$ values. Hence, the onset and endpoint of the CIE may not have been recorded at Úrkút. On the other hand, the intense diagenetic alteration of OM (decomposition and formation of carbonate ore) may have caused the carbon isotopic composition of residual OM to shift towards less negative values, as was observed by, for example, Vető et al. (1997); note the slight isotopic shift in the main ore bed.

6. Conclusions

A mineralogical and geochemical multiple proxy study of the Toarcian black shale that hosts a microbially mediated Mn-carbonate ore deposit at Úrkút in central Hungary was undertaken to determine its petrogenesis and paleoenvironmental setting.

The main conclusions are:

1. The Úrkút black shale is a gray shale and lean in organic matter compared to epicontinental black shales.
2. The dominant mineralogical assemblage is authigenic rather than detrital.
3. The depocenter was a starved basin during accumulation of the black shale in the sense of diminished input of mineral detritus.
4. The organic matter content and diagenetic anoxic environment were the result of rapid accumulation of microbial organic matter that resulted from microbial booms accompanied by a geothermally generated hydrothermal circulation system, and the high rate of accumulation of authigenic minerals (clay minerals and proto-ore minerals). The organic matter was trapped and degraded in a suboxic–anoxic diagenetic environment where pyrite was produced, decreasing the abundance of organic matter.
5. The sharp contact between the limestone/marlstone footwall and black shale unit Bs1 and the Mn-ore deposit reflects the initiation of a hydrothermal vent system in the marine basin. The inferred enzymatic Mn and Fe oxidation blocked carbonate formation by decreasing pH.
6. Even though Mn-oxide accumulation started very close to the contact with the underlying unit, accumulation of proto-ore did not initially predominate probably because of oxygen deficiency, because Mn(II) enzymatic oxidation is obligatory to this process. But the system remained suboxic via syngenetic mineral accumulation (Fe-rich biomats), and became anoxic through diagenesis.
7. The separation of black shale beds and ore beds is not distinct throughout the section. Instead, the distal part of a hydrothermal system promoted the formation of a clay mineral-rich authigenic assemblage (marlstone), which best describes the black shale, in which distinct Mn-oxide proto-ore beds (Mn-rich laminae) formed from nearly the beginning of black shale deposition. Mn-oxide proto-ore transformed into Mn carbonate ore via microbially mediated processes during early diagenesis. Ore beds resulted where these Mn-rich laminae in the BS were highly enriched and abundant.
8. The drivers of Mn-bearing, relatively low organic matter, marlstone formation, compared to other Torcian black shales, were most probably a combination of regional and local processes. Generation of a tectonic rift system promoted geothermally generated circulation cells and hydrothermal fluids and also initiated microbial blooms. The TR and other regions of the Tethyan realm supported formation of black shales under this complex set of processes. These black shale-hosted Mn-carbonate deposits are indicators of ancient failed rift systems.
9. The Úrkút black shale and Mn-ore paleoenvironmental proxies are very similar. Mineralogy, geochemistry, and organic matter are consistent with previous results of the Úrkút, but differ from those of Tethyan epicontinental shelf black shales.

Acknowledgments

The study was supported by the research fund no. 120242 of the National Research Development and Innovation Office, Hungary. S. A. Gerdes and N. Zajzon offered samples, which is highly appreciated. We thank the careful reviews and constructive suggestions provided by Jan Pašava, and the editor.

Appendix A. Supplementary data

Supplementary data to this article can be found online at http://dx.doi.org/10.1016/j.palaeo.2016.06.030.

References

Algeo, T.J., Maynard, J.B., 2004. Trace-element behavior and redox facies in core shales of Upper Pennsylvanian Kansas-type cyclothems. Chem. Geol. 206 (3–4), 289–318.

Andrusov, D., 1965. Geologie der Tschechoslowakischen Karpaten. II. Akad.-Verlag, Berlin (443 pp).

Bárdossy, G., Bottyán, L., Gadó, P., Griger, Á., Sasvári, J., 1980. Automated quantitave phase analysis of bauxites. Am. Mineral. 65, 135–141.

Bargar, J.R., Tebo, B.M., Bergmann, U., Webb, S.M., Glatzel, P., Chiu, V.Q., Villalobos, M., 2005. Biotic and abiotic products of Mn(II) oxidation by spores of the marine *Bacillus* sp. strain SG-1. Am. Mineral. 90, 143–154.

Bassoullet, J.E., Elmi, S., Poisson, A., Cecca, E., Bellion, Y., Guiraud, R., Baudin, E., 1993. Mid Toarcian. In: Dercourt, J., Ricou, L.E., Vrielynck, B. (Eds.), Atlas Tethys Paleoenvironmental Maps. BEICIP-FRANLAB, Rueil-Malmaison.

Bau, M., Dulski, P., 1996. Distribution of yttrium and rare-earth elements in the Penge and Kuruman iron-formations, Transvaal Supergroup, South Africa. Precambrian Res. 79 (1–2), 37–55.

Bau, M., Koschinsky, A., Dulski, P., Hein, J., 1996. Comparison of the partitioning behaviours of yttrium, rare earth elements, and titanium between hydrogenetic marine ferromanganese crusts and seawater. Geochim. Cosmochim. Acta 60 (10), 1709–1725.

Beran, A., Faupl, P., Hamilton, W., 1983. Die Manganschiefer der Strubbergschichten (Nördliche Kalkalpen. Österreich — eine diagenetisch gepragte Mangankarbonatvererzung. TMPM Tscgermaks Min. Petr. Mitt. 31, 175–192.

Bernoulli, D., Jenkyns, H.C., 1974. Alpine, Mediterranean and Central Atlantic Mesozoic Facies in Relation to the Early Evolution of the Tethys. In: Dott, R.H., Shaver, R.H. (Eds.), Modern and Ancient Geosynclinal Sedimentation. SEPM Spec. Publ. 19, pp. 129–187.

Bíró, L., Polgári, M., Tóth, M., Vigh, T., Kávási, N., Sahoo, S.K., 2015. Terrestrial radioisotopes as paleoenvironmental proxies in sedimentary formations. J. Radioanal. Nucl. Chem. 306 (1), 289–293.

Bolhar, R., Kamber, B.S., Moorbath, S., Fedo, C.M., Whitehouse, M.J., 2004. Characterisation of early Archaean chemical sediments by trace element signatures. Earth Planet. Sci. Lett. 222, 43–60.

Bright, C.A., Cruse, A.M., Lyons, T.W., MacLeod, K.G., Glascock, M.D., Ethington, R.L., 2009. Seawater rare-earth element patterns preserved in apatite of Pennsylvanian conodonts? Geochim. Cosmochim. Acta 73, 1609–1624.

Brumsack, H.-J., 2006. The trace metal content of recent organic carbon-rich sediments: implications for Cretaceous black shale formation. Palaeogeogr. Palaeoclimatol. Palaeoecol. 232, 344–361.

Campbell, F.A., Williams, G.D., 1965. Chemical composition of shales of Mannville Group (Lower Cretaceous) of Central Alberta, Canada. AAPG Bull. 49 (1), 81–87.

Channell, J.E.T., Brandner, R., Spieler, A., Stoner, J.S., 1992. Paleomagnetism and paleogeography of the Northern Calcareous Alps (Austria). Tectonics 11 (4), 792–810.

Cora, I., 2009. Mineralogical Study of the Úrkút Mn Carbonate Ore Thesis Eötvös University, Budapest (120 p).

Cornelius, H.P., Plöchinger, B., 1952. Der Tennengebirgs-N-Rand mit seinen Manganerzen und die Berge im Bereich des Lammertales. Jb. Geol. B.-A. 10–225.

Coveney Jr., R.M., Chen, N., 1991. Ni–Mo–PGE–Au-rich ores in Chinese black shales and speculations on possible analogues in the United States. Mineral. Deposita 26, 83–88.

Cseh Németh, J., Grasselly, G., Szabó, Z., 1980. Sedimentary Manganese Deposits of Hungary. In: Varentsov, I.M., Grasselly, G. (Eds.), Geology and Geochemistry of Manganese. Akadémiai Kiadó (Budapest) Vol. 2, pp. 199–221.

Csontos, L., Vörös, A., 2004. Mesozoic plate tectonic reconstruction of the Carpathian region. Palaeogeogr. Palaeoclimatol. Palaeoecol. 210, 1–56.

Deconinck, J.-F., Hesselbo, S.P., Debuisser, N., Averbuch, O., Baudin, E., Bessa, J., 2003. Environmental controls on clay mineralogy of an Early Jurassic mudrock (Blue Lias Formation, southern England). Int. J. Earth Sci. 92, 255–266.

Dera, G., Pellenard, P., Niege, P., Deconinck, J.-F., Puceat, E., Dommergues, J.-L., 2009. Distribution of clay minerals in Early Jurassic peritethyan seas: palaeoclimatic significance inferred from multiproxy comparisons. Palaeogeogr. Palaeoclimatol. Palaeoecol. 271, 39–51.

Duarte, L.V., 1998. Clay minerals and geochemical evolution in the Toarcian–lower Aalenian of the Lusitanian basin (Portugal). Cuadernos de Geol. Ibérica. 24, 69–98.

Dulai, A., Suba, Z., Szarka, A., 1992. Toarcian (lower-Jurassic) organic matter-rich black shale in the Réka-valley, Mecsek Mts. Hungary. Bull. Hung. Geol. Surv. 122 (1), 67–87.

Dupraz, C., Viesscher, P.T., 2005. Microbial lithification in marine stromatolites and hypersaline mats. Trends Microbiol. 13, 429–438.

Dypvik, H., Hams, N.B., 2001. Geochemical facies analysis of fine-grained siliciclastics using Th/U, Zr/Rb and (Zr + Rb) /Sr ratios. Chem. Geol. 181, 131–146.

Ehrlich, H.L., 2015. Geomicrobiology. sixth ed. Marcell Dekker Inc., New York (635 pp).

Espitalié, J., Deroo, G., Marquis, F., 1985. Rock Eval pyrolysis and its applications. Revue de l'Institut Francais du Pétrole (Part I 40, 653–578, Part II 40, 755–784, Part III 41, 73–89).

Farrimond, P., Eglinton, G., Brassell, C., Jenkyns,H.C., 1989. Toarcian anoxic event in Europe: an organic geochemical study. Mar. Pet. Geol. 6, 136–147.

Faupl, P., Beran, A., Hamilton, W., 1982. Erkundung auf Mangan in den Strubbergschichten im Gebiet Golling-Abtenau (Salzburg). Ein Kurzbericht über das Projekt SA 14. Arch. Lagerstforsch. Geol. B-A 2, 171.

Figueiredo, M.M., Martins, A.G., Gamelas, J.A.F., 2012. Characterization of bone and bone-based graft materials using FTIR spectroscopy. In: Theophanides, T. (Ed.), Infrared Spectroscopy - Life and Biomedical Sciences. InTech. http://dx.doi.org/10.5772/36379.

Fortin, D., Ferris, F.G., Beveridge, T.J., 1997. Surface-mediated mineral development by bacteria. In: Banfield, J., Nealson, K.H. (Eds.), Geomicrobiology: Interactions Between Microbes and Minerals: Mineralogical Society of America. Rev. Miner. 35, pp. 162–180.

Géczy, B., 1973. The Lower Jurassic ammonite faunas of the Southern Bakony (Transdanubia, Hungary). Ann. Univ. Sci. Bp. Sect. Geol. 17, 181–190.

Germann, K., 1971. Mangan-Eisen-führende Knollen und Krusten in jurassischen Rotkalken der Nördlichen Kalkalpen. N. Jb. Geol. Paläont. Mh. 3, 133–156.

Germann, K., Waldvogel, F., 1971. Mineralparagenesen und Metallgehalte der "Manganschiefer" (unteres Toarcian) in den Allgau-Schichten der Allgauer und Lechtaler Alpen. N. Jb. Geol. Paläont. (Abh.) 139, 316–345.

Glotch, T.D., Rossman, G.R., 2009. Mid-infrared reflectance spectra and optical constants of six iron oxide/oxyhydroxide phases. Icarus 204, 663–671.

Gruss, H., 1956. Exhalativ-sedimentare Mangankarbonatlagerstatten mit besonderer Berücksichtingung der liassichen Vorkommen in den Berchtesgadener und Salzburger Alpen. N. Jhb. Min. Abh. 92, 47–107.

Haas, J., 1994. Mesozoic. University Book. Eötvös Publishing House, Budapest (119 pp).

Haas, J., 2012. Influence of global, regional, and local factors on the genesis of the Jurassic manganese ore formation in the Transdanubian Range. Hungary. Ore Geol. Rev. 47, 77–86.

Hallam, A., 1967. Sedimentology and palaeogeographic significance of certain red limestones and associated beds in the Lias of the Alpine region. Soc. J. Geol. 3, 195–220.

Hallam, A., 1981. A revised sea-level curve for the early Jurassic. Soc. J. Geol. 138, 735–743.

Hámor-Vidó, M., 2015. Observation of Early Diagenetic Processes through Organic Matter Changes in the Toarcian Úrkút Manganese Formation in Hungary. 2015 ICCP Symposium on "Coal and Organic Petrology". In: Kus, J., David, P., Kalaitzidis, S., Schulz, H.-M., Sachsenhofer, R.F. (Eds.), ICCP Program & Abstract Book. 67th Annual Meeting of the International Committee for Coal and Organic Petrology, September 5–11. 2015 Potsdam, Germany. Schriftenreihe der Deutschen Gesellschaft für Geowissenschaften Heft. 87, p. 88.

Hesselbo, S.P., Gröcke, D.R., Jenkyns, H.C., Bjerrum, C.J., Farrimond, E., Morgans Bell, H.S., Green, O.R., 2000. Massive dissociation of gas hydrate during a Jurassic oceanic anoxic event. Nature 406, 392–395.

Hollander, D.J., Bessereau, G., Belin, S., Hue, A.Y., Houzay, J.P., 1991. Organic matter in the early Toarcian shales, Paris Basin, France: a response to environmental changes. Revue de l'Institut Français du Pétrole. 46 (5), 543–562.

Jach, R., Dudek, T., 2005. Origin of a Toarcian manganese carbonate/silicate deposit from the Krížna unit, Tatra Mountains. Poland. Chem. Geol. 224, 136–152.

Jenkyns, H.C., 1985. The early Toarcian and Cenomanian–Turonian anoxic events in Europe: comparisons and contrasts. Geol. Rundsch. 74 (3), 505–518.

Jenkyns, H.C., 1988. The early Toarcian (Jurassic) anoxic event: stratigraphy, sedimentary, and geochemical evidence. Am. J. Sci. 288, 101–151.

Jenkyns, H.C., 2010. Geochemistry of oceanic anoxic events. Geochem. Geophys. Geosyst. 11 (3), 1–30.

Jenkyns, H.C., Clayton, C.J., 1997. Lower Jurassic epicontinental carbonates and mudstones from England and Wales: chemostratigraphic signals and the early Toarcian anoxic event. Sedimentology 44, 687–706.

Jenkyns, H.C., Géczy, B., Marshall, J.D., 1991. Manganese deposits of central Europe and the Early Toarcian anoxic event. J. Geol. 99, 137–150.

Jenkyns, H.C., Gröcke, D.R., Hesselbo, S.E., 2001. Nitrogen isotope evidence for water mass denitrification during the early Toarcian (Jurassic) anoxic event. Paleoceanography 16, 593–603.

João, T.-A., Dirkx, R., Veld, H., Klaver, G., De Boer, P.L., 2012. Toarcian black shales in the Dutch Central Graben: record of energetic, variable depositional conditions during an Oceanic Anoxic Event. J. Sediment. Res. 82, 104–120. http://dx.doi.org/10.2110/jsr.2012.5.

Katz, B.J., 1994. The Schistes Carton — the Lower Toarcian of the Paris Basin. In: Katz, B.J. (Ed.), Petroleum Source Rocks. Springer-Verlag, Berlin-Heidelberg-New York, pp. 51–65.

Kázmér, M., Kovács, S., 1985. Permian-Paleogene paleogeography along the eastern part of the Insubric-Periadriatic lineament system: evidence for continental escape of the Bakony-Drauzug unit. Acta Geol. Hung. 28, 71–84.

Kearey, P., 2001. The New Penguin Dictionary of Geology. Penguin, London, p. 30.

Kemp, D.B., Coe, A.L., Cohen, A.S., Schwark, L., 2005. Astronomical pacing of methane release in the Early Jurassic period. Nature 423, 396–399.

Kemp, D.B., Kentaro Izumi, K., 2014. Multiproxy geochemical analysis of a Panthalassic margin record of the early Toarcian oceanic anoxic event (Toyora area, Japan). Palaeogeogr. Palaeoclimatol. Palaeoecol. 414, 332–341.

Konhauser, K. (Ed.), 2012. Fundamentals of Geomicrobiology. Wiley-Blackwell Science Ltd., pp. 50–210.

Konhauser, K., 1998. Diversity of bacterial iron mineralization. Earth Sci. Rev. 43, 91–121.

Krainer, K., Mostler, H., Haditsch, J.G., 1994. Jurassische Beckenbildung in den Nördlichen Kalkalpen bei Lofer (Salzburg) unter besonderer Berücksichtigung der Manganerz-Genese. Abh. Geol. B-A 50, 257–293.

Krajewsky, K.P., Lefeld, J., Lacka, B., 2001. Early diagenetic processes in the formation of carbonate-hosted Mn ore deposit (Lower Jurassic, Tatra Mountains) as indicated from its carbon isotopic record. Bull. Pol. Acad. Sci. 49 (1), 13–29.

Küspert, W., 1982. Environmental Changes during Oil Shale Deposition as Deduced from Stable Isotope Ratios. In: Einsale, G., Seilacher, A. (Eds.), Cyclic and Event Stratification. Springer-Verlag, New York, pp. 482–501.

Loukola-Ruskeeniemi, K., 1999. Origin of black shales and the serpentinite-associated Cu–Zn–Co ores at Outokumpu. Finland. Econ. Geol. 94, 1007–1028.

Madejová, J., Komadel, P., 2001. Baseline studies of the clay minerals society source clays: infrared methods. Clay Clay Miner. 49, 410–432.

McArthur, J., Algeo, T., van de Schottbrugge, B., Li, Q., Howarth, R., 2008. Basinal restriction, black shales, Re–Os dating, and the Early Toarcian (Jurassic) oceanic anoxic event. Paleoceanography 23, 1–22. http://dx.doi.org/10.1029/2008PA001607 (PA4217).

Milota, K., 1992. Geochemistry and Interpretation of Hydrocarbons of Mesozoic Formations of Mecsek-Nagykőrös-Debrecen zone According to Aspects of Raw Material Exploration Thesis University of Szeged (96 p).

Molnár, Z., 2015. Initial Fe–Mn-oxide ore indications in the footwall of the Toarcian Úrkút Mn-carbonate ore deposit, Hungary Thesis Eötvös University, Budapest (208 p).

Morris, K.A., 1980. Comparison of major sequences of organic-rich mud deposition in the British Jurassic. Soc. J. Geol. 137, 157–170.

Müller, C.M., Pejcic, B., Esteban, L., Delle Piane, C., Raven, M., Mizaikoff, B., 2014. Infrared attenuated total reflectance spectroscopy: an innovative strategy for analyzing mineral components in energy relevant systems. Sci. Report. http://dx.doi.org/10.1038/srep06764 (4, Article number: 6764).

Nesbitt, H.W., Young, G.M., 1982. Early Proterozoic climates and plate motions inferred from major element chemistry of lutites. Nature 199, 715–717.

Neuendorf, K.K.E., Mehl, J.P.J., Jackson, J.A. (Eds.), 2005. Glossary of Geology, Alexandria, Va, fifth ed. Am. Geol. Inst, p. 72.

Nothdruft, L.D., Gregory, E.W., Balz, S.K., 2004. Rare earth element geochemistry of Late Devonian reefal carbonates, Canning Basin, Western Australia: confirmation of a seawater RFF proxy in ancient limestones. Geochim. Cosmochim. Acta 68 (2), 263–283.

Pace, A., Bouton, A., Bourillot, R., Vennin, E., Visscher, P., Dupraz, C., Thomazo, C., Galaup, S., Kwasniewski, A., 2015. Microbial and Physicochemical Steps Leading to the Mineralization of the Great Salt Lake Microbialites. Abstract Volume. Goldschmidt Conference (No. 2374).

Pálfy, J., Smith, E.L., 2000. Synchrony between Early Jurassic extinction, oceanic anoxic event, and the Karoo-Ferrar flood basalt volcanism. Geology 28 (8), 747–750.

Pálfy, J., Smith, E.L., Mortensen, J.K., 2002. Dating the end-Triassic and Early Jurassic mass extinctions, correlative large igneous provinces, and isotopic events, in: Koeberl, C., Macleod, K.G. (Eds), Catastrophic Events & Mass Extinctions. Impacts and Beyond. Geol. Soc. Am. Spec. Pap. 356, 523–532.

Parikh, S.J., Chorover, J., 2006. ATR-FTIR spectroscopy reveals bond formation during bacterial adhesion to iron oxide. Langmuir 22 (20), 8492–8500.

Pašava, J., 1993. Anoxic sediments — an important source for PGE; an overview. Ore Geol Review 8, 425–445.

Pekker, P., 2005. Mineralogy of the Eplény Limestone Formation, Úrkút Hungary Thesis Eötvös University, Budapest, pp. 3–55.

Polák, S., 1957. Manganese ores of the Malé Karpaty Mts. Geol. práce Zos. 47, 39–83.

Polgári, M., 1993. Manganese Geochemistry Reflected by Black Shale Formation and Diagenetic Processes — Model of Formation of the Carbonatic Manganese Ore of Úrkút. Special Series of Hungarian Geological Institute. Karpati Publish House, Ushgorod. 211 pp.

Polgári, M., 2001. Contribution of volcanic material? – A new aspect of the genesis of the black shale-hosted Jurassic Mn-carbonate ore formation, Úrkút Basin. Hungary. Acta Geol. Hung. 44 (4), 419–438.

Polgári, M., Bajnóczi, B., Kis, V.K., Gotze, J., Dobosi, G., Tóth, M., Vígh, T., 2007. Mineralogical and cathodoluminescence characteristics of Ca-rich kutnohorite from the Úrkút Mn-carbonate mineralization. Hungary. Miner. Mag. 71 (5), 493–508.

Polgári, M., Bíró, L., Pál-Molnár, E., Dobosi, G., Bajnóczi, B., Németh, T., Kovács Kis, V., Vígh, T., 2013b. Rhodochrosite-bearing concretions from a Jurassic Manganese ore mineralization, Úrkút. Hungary. Carpathian J. Earth Envir. Sci. 8 (4), 139–146.

Polgári, M., Dobosi, G., Horváth, P., Rálischné Felgenhauer, E., Vigh, T., 2003a. As-bearing pyrite at Úrkút and in the Jurassic layers of borehole Iharosberény-I. Bull. Hung. Geol. Surv. 133 (4), 69–475.

Polgári, M., Hein, J.R., Németh, T., Pál-Molnár, E., Vigh, T., 2013a. Celadonite and smectite formation in the Úrkút Mn-carbonate ore deposit (Hungary). Sediment. Geol. 294, 157–163.

Polgári, M., Hein, J.R., Tóth, A.L., Pál-Molnár, E., Vígh, T., Bíró, L., Fintor, K., 2012b. Microbial action formed Jurassic Mn-carbonate ore deposit in only a few hundred years (Úrkút, Hungary). Geology 40 (10), 903–906.

Polgári, M., Hein, J.R., Tóth, M., Brukner-Wein, A., Vígh, T., Bíró, L., Cserháti, C., 2010. Genesis of a regionally widespread celadonitic chert ironstone bed overlying upper Lias manganese deposits. Hungary. Soc. J. Geol. 167 (2), 313–328.

Polgári, M., Hein, J.R., Vigh, T., Szabó-Drubina, M., Fórizs, I., Bíró, L., Müller, A., Tóth, L., 2012a. Microbial processes and the origin of the Úrkút manganese deposit. Hungary. Ore Geol. Rev. 47, 87–109.

Polgári, M., Molák, B., Surova, É., 1992. An organic geochemical study to compare Jurassic black shale-hosted manganese carbonate deposits: Úrkút, Hungary, and Branisko Mountains. East Slovakia. Explor. Mining Geol. 1 (1), 63–67.

Polgári, M., Németh, T., Pál-Molnár, E., Futó, I., Vigh, T., Mojzsis, J.S., 2016. Correlated chemostratigraphy of Mn-carbonate microbialites (Úrkút, Hungary). Gondwana Res. 29 (1), 278–289.

Polgári, M., Okita, P.M., Hein, J.R., 1991. Stable isotope evidence for the origin of the Úrkút manganese ore deposit. Hungary. J. Sed. Petrol. 61 (3), 384–393.

Polgári, M., Szabó, Z., Szabó-Drubina, M., Hein, R.J., Yeh, H.W., 2005. A porous silica rock ("Tripoli") in the footwall of the Jurassic Úrkút manganese deposit, Hungary: composition, and origin through carbonate dissolution. Sediment. Geol. 177 (1-2), 87–96.

Polgári, M., Szabó, Z., Szederkényi, T. (Eds.), 2000. Manganese Ores in Hungary — In Commemoration of Professor Gyula Grasselly – Hungarian Academy of Sciences. Juhász Publishing House, Szeged (675 pp).

Polgári, M., Szabó-Drubina, M., Hein, J.R., 2003b. Phosphogenesis in Jurassic black shale-hosted Mn-carbonate deposits, Úrkút and Eplény, Hungary: investigations on archive sample drillcore Úrkút-136. Bull. Hung. Geol. Surv. 133 (1), 37–48.

Polgári, M., Szabó-Drubina, M., Szabó, Z., 2004. Theoretical model for the Mid-European Jurassic Mn-carbonate mineralization Úrkút. Hungary. Bull. Geosci. 79 (1), 53–61.

Rantitsch, G., Melcher, F., Meisel, T., Rainer, T., 2003. Rare earth, major and trace elements in Jurassic manganese shales of the Northern Calcareous Alps: hydrothermal, versus hydrogenous origin of stratiform manganese deposits. Mineral. Petrol. 77 (1–2), 109–127.

Raucsik, B., Merényi, L., 2000. Origin and environmental significance of clay minerals in the Lower Jurassic formations of the Mecsek Mts. Hungary. Acta Geol. Hung. 43 (4), 405–429.

Raucsik, B., Varga, A., 2008a. Mineralogy of the Lower Toarcian black shale section from the Réka Valley (Óbánya Siltstone Formation, Mecsek Mountains, Hungary): implications for palaeoclimate. Bull. Hung Geol Surv. 138 (2), 133–146.

Raucsik, B., Varga, A., 2008b. Climato-environmental controls on clay mineralogy of the Hettangial-Bajocian successions of the Mecsek Mountains, Hungary: an evidence for extreme continental weathering during the early Toarcian oceanic anoxic event. Palaeogeogr. Palaeoclimatol. Palaeoecol. 265 (1), 1–13.

Röhl, H.J., Schmid-Röhl, A., Oschmann, W., Frimmel, A., Schwark, L., 2001. The Posidonia Shale (Lower Toarcian) of SW-Germany: an oxygen-depleted ecosystem controlled by sea level and palaeoclimate. Palaeogeogr. Palaeoclimatol. Palaeoecol. 165, 27–52.

Rosales, I., Quesada, S., Robles, S., 2004. Paleotemperature variations of Early Jurassic seawater recorded in geochemical trends of belemnites from the Basque-Cantabrian basin, northern Spain. Palaeogeogr. Palaeoclimatol. Palaeoecol. 203, 253–275.

Roy, S., 1981. Manganese Deposits. Academic Press, London (458 pp).

Sælen, G., Tyson, R.V., Telwes, N., Tabot, M.R., 2000. Contrasting watermass conditions during deposition of the Whitby Mudstone (Lower Jurassic) and Kimmeridge Clay (Upper Jurassic) formations, UK. Palaeogeogr. Palaeoclimatol. Palaeoecol. 163, 163–196.

Scheffler, K., 2004. Reconstruction of Sedimentary Environment and Climate Conditions by Multi-geochemical Investigations of Late Palaeozoic Glacial to Postglacial Sedimentary Sequences from SW-Gondwana PhD Thesis Rheinischen Friedrich-Wilhelms-Universität Bonn, Wuppertal, Bonn, Germany, p. 243.

Schmid-Röhl, A., Röhl, H.J., Oschmann, W., Frimmel, A., Schwark, L., 2002. Paleoenvironmental reconstruction of Lower Toarcian epicontinental black shales (Posidonia Shale, SW Germany): global versus regional control. Geobios 35, 13–20.

Schmitz, B., Charisi, S.D., Thompson, E.I., Speijer, R.P., 1996. Barium, SiO_2 (excess), and P_2O_5 as proxies of biological productivity in the Middle East during the Paleocene and the latest Paleocene benthic extinction events. Terra Nova 9 (2), 95–99.

Schwark, L., Frimmel, A., 2004. Chemostratigraphy of the Posidonia Black Shale, SW-Germany: II. Assessment of extent and persistence of photic-zone anoxia using aryl isoprenoid distributions. Chem. Geol. 206 (3-4), 231–248.

Song, H., Wignall, P.B., Tong, J., Bond, D.P.G., Song, H., Lai, X., Zhang, K., Wang, H., Chen, Y., 2012. Geochemical evidence from bio-apatite for multiple oceanic anoxic events during Permian–Triassic transition and the link with end-Permian extinction and recovery. Earth Planet. Sci. Lett. 353–354, 12–21.

Szabó, Z., Grasselly, G., 1980. Genesis of Manganese Oxide Ore in the Úrkút Basin, Hungary. In: Varentsov, I.M., Grasselly, G. (Eds.), Geology and Geochemistry of Manganese Vol. 2. Akadémiai Kiadó, Budapest, pp. 223–236.

Szabó-Drubina, M., 1959. Manganese deposits of Hungary. Econ. Geol. 54, 1078–1093.

Taylor, H., Teichmüller, M., Davis, A., Diessel, C.F.K., Littke, R., Robert, P., 1998. Organic Petrology. Borntraeger, Berlin-Stuttgart (704 pp).

Taylor, S.R., McLenmann, S.M., 1995. The geochemical evolution of the continental crust. Rev. Geophys. 33, 241–265.

Tebo, B.M., Bargar, J.R., Clement, B., Dick, G., Murray, K.J., Parker, D., Verity, R., Webb, S., 2004. Manganese biooxide: properties and mechanisms of formation. Annu. Rev. Earth Planet. Sci. 32, 287–328.

Toth, J.R., 1980. Deposition of submarine crusts rich in manganese and iron. Geol. Soc. Am. Bull. 91, 44–54.

Tóth, E., Weiszburg, G.T., Jeffries, T., Williams, C.T., Bartha, A., Bertalan, É., Cora, I., 2010. Submicroscopic accessory minerals overprinting clay mineral REE patterns (celadonite–glauconite group examples). Chem. Geol. 269, 312–328.

van de Schootbrugge, B., Bailey, T.R., Rosenthal, Y., Falkowski, P.G., Katz, M.E., Wright, J.D., Miller, K.G., Feist-Burkhardt, S., 2005. Early Jurassic climate change and the radiation of organic-walled phytoplankton in the Tethys Ocean. Paleobiology 1–19.

Varga, A., Raucsik, B., Hámor-Vidó, M., Rostási, Á., 2007. Isotope geochemistry and characterization of hydrocarbon potential of black shale from Óbánya Siltstone Formation. Bull. Hung. Geol. Surv. 137 (4), 449–472.

Vető, I., 1993. Quantitative investigation of effect of anaerobic bacterial degradation of organic matter of marine sedimentary rocks. Doctor thesis, manuscript. Manuscript Archive. Hungarian Academy of Sciences (D/16.918. 85 pp).

Vető, I., Demény, A., Hertelendi, E., Hetényi, M., 1997. Estimation of primary productivity in the Toarcian Tethys — a novel approach based on TOC, reduced sulphur and manganese contents. Palaeogeogr. Palaeoclimatol. Palaeoecol. 132, 355–371.

Vető, I., Hetényi, M., Demény, A., Hertelendi, E., 1995. Hydrogen index as reflecting intensity of sulphidic diagenesis in non-bioturbated shaly sediments. Org. Geochem. 22 (2), 299–310.

Webb, S., Dick, G.J., Bargar, J.R., Tebo, B.M., 2005. Evidence for the presence of Mn (III) intermediates in the bacterial oxidation of Mn(II). Microbiology 102, 5558–5563.

Wedepohl, K.H., 1971. Environmental Influences on the Chemical Composition of Shales and Clays. In: Ahrens, L.H., Press, F., Runcorn, S.K., Urey, H.C. (Eds.), Physics and Chemistry of the Earth 8. Pergamon, Oxford, pp. 307–331.

Weiszburg, T.G., Nagy, T., Tóth, E., Mizák, J., Varga, Z., Lovas, Gy., A., Váczi, T., 2004a. A laboratory procedure for separating micas from quartz in clay-sized materials. Acta Mineral. Petrogr. Szeged. 45 (1), 133–139.

Weiszburg, T.G., Tóth, E., Beran, A., 2004b. Celadonite, the 10-Å green clay mineral of the manganese carbonate ore, Úrkút Hungary. Acta Mineral. Pet. Szeged. 45 (1), 65–80.

Wignall, P.B., 1994. Black Shales. Clarendon Press, Oxford (124 pp).

Wignall, P.B., Newton, R.J., Little, C.T.S., 2005. The timing of paleoenvironmental change and cause-and-effect relationships during the Early Jurassic mass extinction in Europe. Am. J. Sci. 305, 1014–1032.
Yang, B., Hu, B., Bao, Z., Zhang, Z., 2011. RFF geochemical characteristics and depositional environment of the black shale-hosted Baiguoyuan Ag–V deposit in Xingshan, Hubei Province. China. J. Rare Earths. 29 (5), 499–506.
Yeshaya, B.-O., Moshe, S., 1988. The role of cell-bound flocculants in coflocculation of benthic cyanobacteria with clay particles. FEMS Microbiol. Lett. 53 (3–4), 169–174.
Zavarzin, G.A., 2003. Diversity of Cyanobacterial Mats. In: Krumbein, W.E. (Ed.), Fossil and Recent Biofilms. 8, pp. 141–150.